

RAMP3 determines rapid recycling of atypical chemokine receptor-3 for guided angiogenesis

Classification: Biological Sciences- Cell Biology

Authors: Duncan I. Mackie^a, Natalie R. Nielsen^a, Matthew Harris^b, Smriti Singh^a, Reema B. Davis^a, Danica Dy^a, Graham Ladds^b, and Kathleen M. Caron^{a*}

Affiliations:

^aDepartment of Cell Biology and Physiology, University of North Carolina, Chapel Hill, North Carolina, 27599.

^bDepartment of Pharmacology, University of Cambridge, Cambridge, CB2 1PD, United Kingdom.

Corresponding Author:

***Kathleen M. Caron, PhD**

111 Mason Farm Road; CB# 7545

6312B Medical Biomolecular Research Building

Chapel Hill, NC 27599

Fax: 919-843-1316 Tele: 919-843-5193

Kathleen_caron@med.unc.edu

Abstract

Receptor activity-modifying proteins (RAMPs) are single transmembrane spanning proteins which serve as molecular chaperones and allosteric modulators of G protein coupled receptors (GPCRs) and their signaling pathways. Although RAMPs have been previously studied in the context of their effects on Family B GPCRs, the coevolution of RAMPs with many GPCR families suggests an expanded repertoire of potential interactions. Using BRET-based and cell surface expression approaches, we comprehensively screen for RAMP interactions within the chemokine receptor family and identify robust interactions between RAMPs and nearly all chemokine receptors. Most notably, we identify robust RAMP interaction with atypical chemokine receptors (ACKRs), which function to establish chemotactic gradients for directed cell migration. Specifically, RAMP3 association with atypical chemokine receptor 3 (ACKR3) diminishes adrenomedullin (AM) ligand availability without changing G protein coupling. Instead, RAMP3 is required for the rapid recycling of ACKR3 to the plasma membrane through Rab4-positive vesicles following either AM or SDF-1/CXCL12 binding, thereby enabling formation of dynamic spatiotemporal chemotactic gradients. Consequently, genetic deletion of either ACKR3 or RAMP3 in mice abolishes directed cell migration of retinal angiogenesis. Thus, RAMP association with chemokine receptor family members represents a novel molecular interaction to control receptor signaling and trafficking properties.

Key Words: Chemokine Receptors, G Protein-Coupled Receptors, Angiogenesis

Significance Statement: G protein coupled-receptors (GPCRs) exist within multi-protein complexes on the surface of cells in order to respond to a wide variety of extracellular stimuli such as neurotransmitters, migratory cues, hormones, light and odors. In this study, we discover and characterize an expanded repertoire of GPCRs that interact with receptor activity modifying proteins (RAMPs)—a class of proteins that can modulate the type and consequences of extracellular signals to GPCRs. Specifically, we find that RAMP interaction with chemokine

GPCRs is essential for enabling these receptors to bind and degrade extracellular migratory cues and thereby establish gradients for directed cellular migration. In the absence of these critical proteins, the process of blood vessel sprouting within the postnatal retina is dysfunctional.

Introduction

RAMPs are a family of single-pass transmembrane proteins with 3 mammalian members: RAMP1, RAMP2 and RAMP3, each encoded by a distinct and corresponding gene (1-3). The RAMPs were first identified by virtue of their requirement for promoting the forward translocation of calcitonin receptor-like receptor (CLR) from the cytoplasm to the plasma membrane (3). Moreover, their association with this receptor imparts ligand binding specificity, such that a RAMP1-CLR oligomer preferentially binds the neuropeptide, calcitonin gene related peptide (CGRP), whilst the RAMP2-CLR or RAMP3-CLR oligomers display higher affinity for a related vasodilatory peptide, adrenomedullin (AM). Recent cryo-EM resolution of the molecular interaction between RAMP1 and calcitonin receptor-like receptor (CLR) exemplifies how RAMPs impart ligand binding specificity (4), which has been exploited in the design of the first FDA-approved antibody-based therapy against a GPCR for the treatment of migraine (5). Subsequent studies have further defined critical roles for RAMPs to impart biased downstream signaling and intracellular trafficking dynamics to numerous G protein-coupled receptors (GPCRs). However, these pleiotropic effects of RAMPs have mostly been studied in the context of a few receptors in the Family B/Secretin family, including calcitonin receptor (CTR), secretin receptor, glucagon (6, 7), CRF₁ (8, 9) and VPAC_{1/2} (8) and the Family A receptors, CaSR,(10) and GPR30/GPER1(11). The strong co-evolution of RAMPs with most GPCR families suggests that they may have expanded interacting partners (12, 13).

The chemokine receptor subfamily is comprised of 24 different GPCRs that each bind a diverse array of chemokine and peptide ligands, leading to a wide variety of signaling events and physiological functions, ranging from innate immunity, developmental chemotaxis, HIV infection to cancer metastasis (14-16). The redundancy of ligands binding to multiple chemokine receptors underscores the importance, and also the complexity, of chemokine signaling. As one example, the establishment of extracellular chemokine gradients for directed cell migration relies on the

concerted, spatiotemporal functions of both typical signaling chemokine receptors with atypical chemokine receptors (ACKRs), sometimes referred to as “decoy” receptors (17). Unlike typical chemokine receptors which elicit a downstream signaling pathway in response to ligand, ACKRs do not signal through G proteins but rather bind and degrade ligands rapidly from the extracellular milieu. Considering this high level of complexity in ligand binding and signaling, we hypothesized that RAMPs may interact with chemokine receptors to modulate their complex signaling, trafficking, and physiological properties. Here, we developed a multimodal screening platform which identified robust interactions between RAMPs and the family of chemokine receptors. We further find that RAMPs play essential roles in determining the internalization, trafficking and recycling of ACKR3, ultimately influencing guided angiogenesis in the postnatal retina.

Results

Identification of chemokine receptor: RAMP interactions using BRET and FACS

We established a bioluminescence resonance energy transfer (BRET)-based screening platform to identify RAMP-GPCR protein interactions by transiently co-expressing a constant amount of GPCR-rLuc protein with increasing amounts of RAMP-YFP protein in HEK293T cells. The canonical RAMP-interacting receptor, CLR, was used as a positive control and the non-interacting beta-2 adrenergic receptor (β_2 ADR) served as a negative control in order to empirically establish a systematic and multi-variate process for identifying and scoring RAMP:GPCR interactions. To evaluate each interaction, the first major discriminator applied was a threshold of $B_{\max} > 0.100$ (**Fig. 1 and SI Appendix, Table S1**). All potential interactions failing to reach this minimum signal level were deemed negative, as indicated by red shading. Next, we applied a best-fit comparison for linearity versus hyperbolic curve fitting for all curves with a $B_{\max} > 0.100$. Interactions with a linearity R^2 greater than the hyperbolic R^2 were considered poor, indicated by yellow shading. Finally, the remaining curves which satisfied the hyperbolic curve fit test were further divided based on their $BRET_{50}$ values. Hyperbolic curves with a $BRET_{50} > 10$ were

considered good interactions and colored blue, whilst curves with $BRET_{50} < 10$ were considered the strongest possible candidates and shaded green. All chemokine receptors exhibited interactions with at least one RAMP. RAMP3 interactions were the most frequent and strongest (24/24 receptors), followed by RAMP2 (20/24) and RAMP1 (15/24) (**Fig. 1**).

Flow cytometry was performed as an orthogonal assay to verify if BRET-based protein-protein interactions translated to effects on RAMP surface expression upon cotransfection with each receptor (**SI Appendix, Fig. S1A**). In the absence of a GPCR, FLAG- and HA-RAMP1 and RAMP2 displayed minimal plasma membrane expression, indicative of endogenous intracellular localization. Both FLAG- and HA-RAMP3 exhibited endogenous plasma membrane expression, an effect also observed in previous studies (18). Importantly, RAMP3 plasma membrane expression could be further enhanced by coexpression with CLR or CTR. CCR5, CXCR2, CX3CR1 and CMKLR1 exhibited highly significant RAMP interactions in both BRET-based and cell surface expression assays. Interestingly, we noticed that three of the members of the subfamily of confirmed atypical chemokine receptors (ACKR1-3, but not ACKR4) interacted robustly with RAMP3 and unlike RAMP1/2, reduced RAMP3 cell surface expression compared to RAMP3 expressed alone. To confirm that the observed effects on RAMP cell surface expression were not due to overexpression, FLAG-RAMPs were titrated with a fixed concentration of receptor. We observed a saturable level of cell surface expression above vector alone for FLAG-RAMP1 with CCR5 and FLAG-RAMP2 with CXCR2, with the plateau corresponding to a 1:1 RAMP:receptor ratio (**SI Appendix, Fig. S1B**). For FLAG-RAMP3, which is able to traffic to the plasma membrane alone, ACKR3 restricted its cell surface expression in a saturable manner. ACKR3 has been reported to more broadly localize to early endosomes prior to ligand stimulation (19). Therefore, a possible explanation for the reduced FLAG-RAMP3 plasma membrane localisation upon coexpression with ACKR3, is that the ACKR3: RAMP3 complex resides largely intracellularly or, alternatively, is targeted for degradation. This mechanism may also apply to

other GPCRs that reduce FLAG-RAMP3 plasma membrane expression. Interestingly, but not unexpectedly, the results from the BRET and FACS experiments reveal some differences in specific RAMP:GPCR interactions. The BRET assay provides a measure of total protein:protein interactions regardless of cellular location, whereas FACS is, one of a number of techniques that measure the extent to which GPCRs alter RAMP expression at the cell surface. Thus, a comparative integration of results for these two methodologies provides the most informed interpretation for the biological functions of these putative RAMP:GPCR interactions.

ACKR3 interacts with RAMP2/3 without affecting G protein or β -Arrestin coupling

We were particularly intrigued by the putative ACKR3:RAMP interaction because, using genetic mouse models, we previously showed that the developmental phenotypes of precocious cardiomyocyte and lymphatic hyperplasia in *Ackr3*^{-/-} mice are attributable to gain-of-function in AM ligand (20), which elicits its signaling through the canonical RAMP-interacting receptor heterodimers, CLR:RAMP2 and CLR:RAMP3. Therefore, we hypothesized that ACKR3 may also utilize RAMPs to modulate its ligand scavenging activities. To address this, we further validated the ACKR3:RAMP3 protein interaction by observing the co-localization of Myc-ACKR3 and HA-RAMP3 at the plasma membrane of non-permeabilized HEK293T cells by confocal microscopy (**Fig. 2A**) and within the cytoplasm by proximity ligation assay (**Fig. 2B**), to an extent similar to that observed for the CLR:RAMP positive controls. Consistent with the established scavenging properties of ACKRs, we used the BRET-based biosensor EPAC (21) to confirm that neither RAMP 1, 2, or 3 could induce activation of G α s (**SI Appendix, Fig. S2A**) nor G α i/o (**SI Appendix, Fig. S2B**) in response to logarithmic dosage of AM or SDF-1/CXCL12 ligands. Furthermore, we did not detect any effects of RAMPs on the AM- or SDF-1/CXCL12-induced recruitment of β -arrestin-1-YFP or β -arrestin-2-YFP to ACKR3-rLuc, as evidenced by non-linear regression best-fit curves of BRET activation (**SI Appendix, Fig. S2C,D**). Both AM and SDF-1/CXCL12 ligand caused the recruitment of β -arrestin-1 and β -arrestin-2 to ACKR3, though SDF-1/CXCL12

showed more efficacy at lower doses than AM (**SI Appendix, Fig. S2C,D**). Collectively, these data establish RAMPs as interacting partners of ACKR3, but these interactions do not influence the downstream G protein or β -arrestin responses of ACKR3 to either AM or SDF-1/CXCL12 ligands.

ACKR3: RAMP3 co-expression scavenges and attenuates AM signaling

We next established cell based cAMP-EPAC reporter assays to distinguish the cell intrinsic and cell autonomous functions of ACKR3 on AM ligand scavenging via activation of the CLR:RAMP3 receptor heterodimer. For example, HEK293T cells transfected with CLR, RAMP3, NSF (N-ethylmaleimide sensitive factor), and the EPAC reporter responded in a dose-dependent manner to AM stimulation ($EC_{50}=1.6 \text{ nM} \pm \log EC_{50}=0.11$, purple circles (**Fig. 3A**)), and this signaling could be significantly attenuated with a large effect at high AM concentrations, evident by the development of a biphasic dose-response curve fit, by the co-transfection of ACKR3 ($EC_{50_1}= 1 \text{ nM} \pm \log EC_{50_1}= 0.20$ and $EC_{50_2}= 3.1 \text{ } \mu\text{M} \pm \log EC_{50_2}= 0.46$, orange squares (**Fig. 3A**)) This was consistent with our previous results showing reduced pERK activation by AM in the presence of ACKR3 (20). Because we found that RAMPs did not induce ACKR3 mediated cAMP production in response to AM (**SI Appendix, Fig. S2A,B**), we reasoned that the reduced potency of AM at the CLR:RAMP3 receptor is caused by reduced bioavailability of AM ligand in the presence of the ACKR3 scavenging receptor. To confirm this, and to provide a model for the cell autonomous scavenging effects of ACKR3 on AM ligand, we employed a co-culture system in which reporter cells expressing CLR:RAMP3:EPAC were co-cultured with cells expressing either ACKR3:RAMP3:NSF or glucagon like peptide 2 receptor (GLP2R), as a non-scavenging control cell (**Fig. 3B**). Upon stimulation with AM, the CLR:RAMP3:EPAC reporter cells co-cultured with the non-scavenging GLP2R-expressing cells stimulated maximal cAMP production with a potency of $0.52 \text{ nM} \pm \log EC_{50}=0.05$ (black circles). In contrast, when the CLR:RAMP3:EPAC reporter cells were co-cultured with ACKR3:RAMP3:NSF-expressing cells, there was a significant

loss in potency to $1.3 \text{ nM} \pm \log EC_{50}=0.08$, as demonstrated by the rightward shift in the dose-response curve (red squares). These data demonstrate the ability of ACKR3:RAMP3 to scavenge AM ligand both in cell intrinsic and cell autonomous settings, thereby attenuating AM signaling and further validating our previous studies using genetic mouse models.

ACKR3 rapid recycling and lysosomal trafficking is dependent upon RAMP3 and NSF

An inherent characteristic for establishing and maintaining chemotactic gradients for guided cell migration within discrete spatiotemporal boundaries, is the rapid and dynamic depletion of extracellular ligands from the non-migrating region (22). Elegant zebrafish studies focused on primordial cell migration in response to SDF-1/CXCL12 gradients have implicated an important function for ACKR3 in this regard (23, 24). However, the molecular partners that enable ACKR3 to rapidly and cell autonomously scavenge ligands from the extracellular compartment remain unknown (25). RAMP3, by virtue of its C-terminal PSD-95/Disks-large/ZO-1 homology (PDZ)-recognition motif associates with N-ethylmaleimide-sensitive factor (NSF). This has previously been shown to facilitate the rapid recycling and resensitization of CLR to the plasma membrane following ligand-dependent internalization (26). Using confocal imaging, we confirmed these original findings for CLR following a 4 hour recovery after removal of AM ligand (**SI Appendix, Fig. S3 and Fig. S4**). Similarly, we found that HEK293T cells transfected with ACKR3, RAMP3 and NSF displayed rapid internalization of ACKR3 following 1 hour of AM ligand stimulation, with subsequent recycling of ACKR3 to the plasma membrane after 4 hours of ligand removal and cycloheximide treatment (**Fig. 3C**, left column and **SI Appendix, Fig. S5**). In contrast, in the absence of either RAMP3 or NSF, although ACKR3 ligand-stimulated internalization occurred at 1 hour, the receptor failed to recycle to the plasma membrane and remained within intracellular vesicles after 4 hour recovery (**Fig. 3C**, middle and right columns and **SI Appendix, Fig. S5**). These data demonstrate the requirement of RAMP3:NSF for the rapid

recycling of the ACKR3 to the plasma membrane where it can evoke its ligand scavenging activities.

Following this same experimental paradigm, we were curious to address whether RAMP3:NSF expression could influence the fate of ACKR3 to different endosomal sorting pathways. To address this, we tracked the ligand-activated internalization of tagged-ACKR3 to fluorescently-labeled, Rab-positive endosomes in the presence or absence of RAMP3:NSF. As shown in **Fig. 4A** (left columns and **SI Appendix, Fig. S6**), ACKR3 rapidly internalized to Rab4-positive vesicles following 1 hour treatment of AM ligand and was subsequently recycled to the plasma membrane after 4 hours recovery in the presence of RAMP3:NSF. Conversely, in the absence of RAMP3:NSF, AM-stimulated ACKR3 internalized to non-Rab4-positive vesicles and never returned to the cell surface (**Fig. 4A**, right columns and **SI Appendix, Fig. S6**). Moreover, when cells were transfected with a GFP-Rab7a lysosomal marker, AM-activated ACKR3 was spared from the lysosomal degradation pathway, and resensitized to the plasma membrane, in the presence of RAMP3:NSF (**Fig. 4B**, left columns and **SI Appendix, Fig. S7**). In the absence of RAMP3:NSF, however, ACKR3 was predominately sorted toward the lysosomal pathway, where its localization within the lumen of Rab7a-positive lysosomes and absence from the plasma membrane was particularly evident 4 hours after AM-stimulation (**Fig. 4B**, right columns and **SI Appendix, Fig. S7**). Importantly, we found the same effects of RAMP3:NSF on ACKR3 sorting when the receptor was activated by SDF-1/CXCL12 (**SI Appendix, Fig. S8, Fig. S9, and Fig. S10**), indicating a ligand-unbiased requirement of RAMP3:NSF for the sorting of ACKR3 to rapidly recycling Rab4-positive endosomes, while being spared from lysosomal degradation.

It has been established that the PDZ recognition sequence in the C' terminal tail of RAMP3 plays a critical role in the recycling of the canonical CLR:RAMP3:NSF complex (26). To test the hypothesis that the RAMP3 type I PDZ recognition motif is a molecular determinate of NSF:ACKR3 receptor trafficking we generated a RAMP3 Δ PDZ expression vector. The deletion

of the PDZ motif (-DTLL) disrupted the ligand-stimulated, selective endosomal sorting of the ACKR3:RAMP3 receptor complex (**SI Appendix, Fig. S11**, for AM ligand and **Fig. S12**, for CXCL12 ligand) irrespective of ligand specificity. Interestingly, we also noted that the receptor complex instead localized to Rab11 slow recycling endosomes, which was previously not detected with wild-type RAMP3.

Loss of guided cell migration in *Ackr3*^{-/-} and *Ramp3*^{-/-} mice during retinal angiogenesis

To determine whether RAMP3-mediated fating of ACKR3 to the rapid recycling endosomal pathway could impact the scavenging properties of the receptor in a physiological context, we turned to postnatal retinal angiogenesis as a model system of guided cell migration (27). In this context, angiogenic cues, like SDF-1/CXCL12 and AM, are enriched within peripheral astrocytes and serve as chemotactic gradients for guided angiogenesis of retinal vasculature by stimulating tip cells and filopodia ((28) and **Fig. 5A,D,G**). Previous studies have defined the presence of ACKR3 within trailing arterioles and concomitantly its notable absence from leading endothelial tip cells within the developing retina, thereby establishing its spatial positioning within the retina to maintain angiogenic gradients (28). Predictably, a 50% reduction in the expression of the scavenging receptor in *Ackr3*^{+/-} animals resulted in a significant reduction in the number of endothelial tip cells within the retinas of postnatal day 3 mice compared to control littermates (**Fig. 5B,E**). Although the vast majority of *Ackr3*^{-/-} mice die at postnatal day 1, we were fortunate to obtain and characterize a single, surviving animal which displayed a profound reduction in tip cell number (**Fig. 5E**) and effacement of the retinal angiogenic front. Importantly, we observed the same attenuation of guided angiogenesis in *Ramp3*^{-/-} animals (29) compared to control littermates (**Fig. 5C,F**). Additionally, we observed a significant decrease in tip cell filopodia in *Ramp3*^{-/-} animals (WT vs *Ramp3*^{-/-}; 20.7 ± 1.34 vs 16.9 ± 0.90 , $p=0.023$) and a trend toward decreased tip cell filopodia in *Ackr3*^{+/-} animals (WT vs *Ackr3*^{+/-}; 24.4 ± 1.45 vs 22.5 ± 1.14 , $p=0.333$). These

findings support an essential physiological function for AM-gradient guided cell migration through the scavenging activities of ACKR3 and RAMP3 (**Fig. 5G**).

Discussion

Collectively, these data significantly expand the repertoire of GPCRs that interact with RAMPs and provide at least one example of how a RAMP:GPCR interaction can dictate the physiological functions of guided cell migration by governing receptor endosomal sorting and recycling (**Fig. 5H**). We focused our efforts on the process of retinal angiogenesis because we, and others, have previously shown that both ACKR3 ligands, SDF-1/CXCL12 and AM, and their respective cognate signaling receptors, CXCR4 and CLR, are critical for driving guided cell migration within this vascular bed (28, 30). However, ACKR3 also plays critical roles in the migration of GABAergic interneurons within the embryonic cerebral cortex (1, 31), in the homing of immune cells to lymphoid tissues and in the migration of cancer cells (32, 33). Thus, it will be of interest to determine whether RAMP3 also dictates the scavenging functions of ACKR3 within these other contexts. If so, the RAMP3-ACKR3 interface should provide a novel therapeutic target for modulating the actions of the CXCR4/CXCL12 axis in anti-cancer and anti-inflammatory strategies (34).

Indeed, the molecular interface formed between RAMP1 and CLR has recently been exploited in the design of the anti-CGRP migraine drug, erenumab (5, 35). In our current study, we find that 23 of the 24 described chemokine receptors display moderate to strong molecular interactions with RAMPs. These findings identify unique and pharmacologically-tractable avenues for the modulation of chemokine function in a wide range of physiological processes. Additional studies that employ a wide range of biochemical, pharmacological, and cellular assays to elucidate the effects that each RAMP has on the ligand binding, biased functional selectivity or trafficking of other chemokine GPCRs provides valuable future exploration and opportunity.

Materials and Methods

Cell culture, Bioluminescence Resonance Energy Transfer (BRET) assays, flow cytometry, immunofluorescence confocal microscopy, whole-mount immunohistochemistry, in situ proximity ligation assay (PLA), receptor scavenging, internalization, resensitization, and trafficking assays performed in this study are provided in SI Appendix, Materials and Methods.

Animals

Adm^{+/hi} and *Ackr3^{+/-}* mice were maintained on a C57BL/6 genetic background and *Ramp3^{-/-}* mice were maintained on a 129/SvEv genetic background. *Ackr3^{-/-}* and *Adm^{hi/hi}* mice were generated by heterozygous intercrosses, respectively. *Ramp3^{-/-}* mice were generated through homozygous crosses of *Ramp3^{-/-}* mice and *Ramp3^{+/+}* isogenic mice were used as controls. A total of 6 mice across two *Adm* genotypes (3 *Adm^{+/+}* and 3 *Adm^{hi/hi}*), 11 mice across the three *Ackr3* genotypes (4 *Ackr3^{+/+}*, 6 *Ackr3^{+/-}*, and 1 *Ackr3^{-/-}*), and 14 mice across two *Ramp3* genotypes (7 *Ramp3^{+/+}* and 7 *Ramp3^{-/-}*) were used in this study. This study was powered to attain statistical significance of $p < 0.05$ with a 90% probability between *Adm^{+/+}* and *Adm^{hi/hi}*, *Ackr3^{+/+}* and *Ackr3^{+/-}*, and *Ramp3^{+/+}* and *Ramp3^{-/-}* mice. All animal procedures and protocols were approved by the UNC-CH Institutional Animal Care and Use Committee.

Acknowledgments

Funding: NIH RO1-DK099156, RO1-HD060860, RO1-HL129086 to K.M.C.; American Heart Association Innovator Award 16IRG27260077 to K.M.C.; NIH F32-HL134279 to D.I.M.; American Heart Association 15POST25270006 to R.B.D.; NIH F31-HL143836 to N.R.N; BBSRC grant BB/M00015X/2 to G.L and BBSRC Doctoral Training Partnership Grant BB/JO14540/1 to M. H.

Data and materials availability: No datasets were generated or analyzed during the current study. All correspondence and material requests should be addressed to Dr. Kathleen M. Caron.

References

1. Saaber F, *et al.* (2019) ACKR3 Regulation of Neuronal Migration Requires ACKR3 Phosphorylation, but Not beta-Arrestin. *Cell reports* 26(6):1473-1488 e1479.
2. Klein KR, Matson BC, & Caron KM (2016) The expanding repertoire of receptor activity modifying protein (RAMP) function. *Critical reviews in biochemistry and molecular biology* 51(1):65-71.
3. McLatchie LM, *et al.* (1998) RAMPs regulate the transport and ligand specificity of the calcitonin-receptor-like receptor. *Nature* 393(6683):333-339.
4. Liang YL, *et al.* (2018) Cryo-EM structure of the active, Gs-protein complexed, human CGRP receptor. *Nature* 561(7724):492-497.
5. Goadsby PJ, *et al.* (2017) A Controlled Trial of Erenumab for Episodic Migraine. *The New England journal of medicine* 377(22):2123-2132.
6. Weston C, *et al.* (2015) Modulation of Glucagon Receptor Pharmacology by Receptor Activity-modifying Protein-2 (RAMP2). *Journal of Biological Chemistry* 290(38):23009-23022.
7. Cegla J, *et al.* (2017) RAMP2 Influences Glucagon Receptor Pharmacology via Trafficking and Signaling. *Endocrinology* 158(8):2680-2693.
8. Wootten D, *et al.* (2013) Receptor activity modifying proteins (RAMPs) interact with the VPAC2 receptor and CRF1 receptors and modulate their function. *British journal of pharmacology* 168(4):822-834.
9. Bailey S, *et al.* (2019) Interactions between RAMP2 and CRF receptors: The effect of receptor subtypes, splice variants and cell context. *Biochimica et biophysica acta. Biomembranes* 1861(5):997-1003.
10. Desai AJ, Roberts DJ, Richards GO, & Skerry TM (2014) Role of receptor activity modifying protein 1 in function of the calcium sensing receptor in the human TT thyroid carcinoma cell line. *PloS one* 9(1):e85237.
11. Lenhart PM, Broselid S, Barrick CJ, Leeb-Lundberg LMF, & Caron KM (2013) G-protein-coupled receptor 30 interacts with receptor activity-modifying protein 3 and confers sex-dependent cardioprotection. *J Mol Endocrinol* 51(1):191-202.
12. Barbash S, Lorenzen E, Persson T, Huber T, & Sakmar TP (2017) GPCRs globally coevolved with receptor activity-modifying proteins, RAMPs. *Proceedings of the National Academy of Sciences of the United States of America* 114(45):12015-12020.
13. Lorenzen E, *et al.* (2019) Multiplexed analysis of the secretin-like GPCR-RAMP interactome. *Science advances* 5(9):eaaw2778.
14. Allen SJ, Crown SE, & Handel TM (2007) Chemokine: receptor structure, interactions, and antagonism. *Annu Rev Immunol* 25:787-820.
15. Blanchet X, Langer M, Weber C, Koenen RR, & von Hundelshausen P (2012) Touch of chemokines. *Frontiers in immunology* 3:175.
16. Hughes CE & Nibbs RJB (2018) A guide to chemokines and their receptors. *The FEBS journal*.
17. Nibbs RJ & Graham GJ (2013) Immune regulation by atypical chemokine receptors. *Nature reviews. Immunology* 13(11):815-829.
18. Christopoulos A, *et al.* (2003) Novel receptor partners and function of receptor activity-modifying proteins. *The Journal of biological chemistry* 278(5):3293-3297.
19. Zhu B, *et al.* (2012) CXCL12 enhances human neural progenitor cell survival through a CXCR7- and CXCR4-mediated endocytotic signaling pathway. *Stem cells* 30(11):2571-2583.
20. Klein KR, *et al.* (2014) Decoy receptor CXCR7 modulates adrenomedullin-mediated cardiac and lymphatic vascular development. *Developmental cell* 30(5):528-540.
21. Barak LS, *et al.* (2008) Pharmacological characterization of membrane-expressed human trace amine-associated receptor 1 (TAAR1) by a bioluminescence resonance energy transfer cAMP biosensor. *Molecular pharmacology* 74(3):585-594.

22. Bussmann J & Raz E (2015) Chemokine-guided cell migration and motility in zebrafish development. *The EMBO journal* 34(10):1309-1318.
23. Venkiteswaran G, *et al.* (2013) Generation and dynamics of an endogenous, self-generated signaling gradient across a migrating tissue. *Cell* 155(3):674-687.
24. Boldajipour B, *et al.* (2008) Control of chemokine-guided cell migration by ligand sequestration. *Cell* 132(3):463-473.
25. Montpas N, *et al.* (2018) Ligand-specific conformational transitions and intracellular transport are required for atypical chemokine receptor 3-mediated chemokine scavenging. *The Journal of biological chemistry* 293(3):893-905.
26. Bomberger JM, Parameswaran N, Hall CS, Aiyar N, & Spielman WS (2005) Novel function for receptor activity-modifying proteins (RAMPs) in post-endocytic receptor trafficking. *The Journal of biological chemistry* 280(10):9297-9307.
27. Rezzola S, *et al.* (2014) In vitro and ex vivo retina angiogenesis assays. *Angiogenesis* 17(3):429-442.
28. Strasser GA, Kaminker JS, & Tessier-Lavigne M (2010) Microarray analysis of retinal endothelial tip cells identifies CXCR4 as a mediator of tip cell morphology and branching. *Blood* 115(24):5102-5110.
29. Dackor R, Fritz-Six K, Smithies O, & Caron K (2007) Receptor activity-modifying proteins 2 and 3 have distinct physiological functions from embryogenesis to old age. *The Journal of biological chemistry* 282(25):18094-18099.
30. Sakimoto S, *et al.* (2013) An angiogenic role for adrenomedullin in choroidal neovascularization. *PloS one* 8(3):e58096.
31. Abe P, *et al.* (2014) CXCR7 prevents excessive CXCL12-mediated downregulation of CXCR4 in migrating cortical interneurons. *Development* 141(9):1857-1863.
32. Hattermann K & Mentlein R (2013) An infernal trio: the chemokine CXCL12 and its receptors CXCR4 and CXCR7 in tumor biology. *Ann Anat* 195(2):103-110.
33. Quinn KE, Mackie DI, & Caron KM (2018) Emerging roles of atypical chemokine receptor 3 (ACKR3) in normal development and physiology. *Cytokine* 109:17-23.
34. Schall TJ & Proudfoot AE (2011) Overcoming hurdles in developing successful drugs targeting chemokine receptors. *Nature reviews. Immunology* 11(5):355-363.
35. Edvinsson L, Haanes KA, Warfvinge K, & Krause DN (2018) CGRP as the target of new migraine therapies — successful translation from bench to clinic. *Nature Reviews Neurology* 14(6):338-350.

Figure Legends

Fig. 1. BRET screening of the chemokine receptor family reveals heterodimers with receptor activity modifying proteins (RAMPs). Δ BRET was determined using HEK293T cells for each receptor: RAMP pair and plotted as a function of the total fluorescence/total luminescence ratio. Curves were calculated using one site binding (hyperbola) and representative saturation isotherms are displayed for each receptor. A systematic, multi-component approach was used to score interactions. First, all interactions failing to reach a requirement of $B_{max} > 0.1$

were deemed negative (red). Next, a comparison of fits between hyperbolic and linear models was used where Linear $R^2 >$ Hyperbolic R^2 was deemed a poor interaction (yellow). Finally, the remaining interactions were deemed good or strong based on the $BRET_{50}$ values, $BRET_{50} > 10$ (blue) or $BRET_{50} < 10$ (green), respectively. Curves are representative of $n=3-4$ independent experiments for each RAMP-receptor interaction, with average data reported in Supplemental Table 1.

Fig. 2. Cellular distribution of ACKR3: RAMP3 and translocation to the plasma membrane.

(A) HEK293T cells transfected with HA-RAMP alone or with Myc-CLR or Myc-ACKR3 as indicated. Addition of CLR and ACKR3 resulted in an increased the detection of GPCR: RAMP at the plasma membrane. HA-tagged RAMP2 and RAMP3 exhibited very low levels of GPCR independent localization. $n=3$ for each condition. (B) Proximity ligation assay (PLA) showed significant increases in signal for CLR with RAMP3 and ACKR3 with RAMP3 when compared with GPCR alone transfected controls. Blue is the nuclear staining and green is beta catenin to stain the membrane. The graph shows the number of PLA signals per cell that correspond to number of associations or heterodimer complexes for GPCR with RAMP3. Each color represents an individual experiment, $n=3$, counting 7-21 individual cells per n . Statistical significance was determined by an unpaired t test. Error bars represent SEM of the means. Scale bar 10 μ m.

Fig. 3. The ACKR3: RAMP3: NSF complex attenuates adrenomedullin signaling and regulates the ACKR3 receptor's rapid recycling.

(A) Expression of ACKR3 in the same HEK293T cells as the CLR: RAMP3 heterodimer resulted in a marked decrease in cAMP EPAC biosensor signal, indicating reduced potency and a resulting biphasic dose-response (EC_{50} for -ACKR3= 1.6 nM, $\pm \log EC_{50}=0.11$ to +ACKR3 $EC_{50_1}= 1$ nM, $\pm \log EC_{50_1}= 0.20$ and $EC_{50_2}= 3.1$ μ M, $\pm \log EC_{50_2}= 0.46$ with Hill slope for -ACKR3= 0.58 ± 0.08 and nHill slope for +ACKR3 $nH1=-0.92 \pm 0.40$ and $nH2=-1.17 \pm 0.99$) (B) Coculturing the CLR: RAMP3: EPAC reporter cells with HEK293T cells expressing ACKR3: RAMP3: NSF resulted in a loss of AM potency as

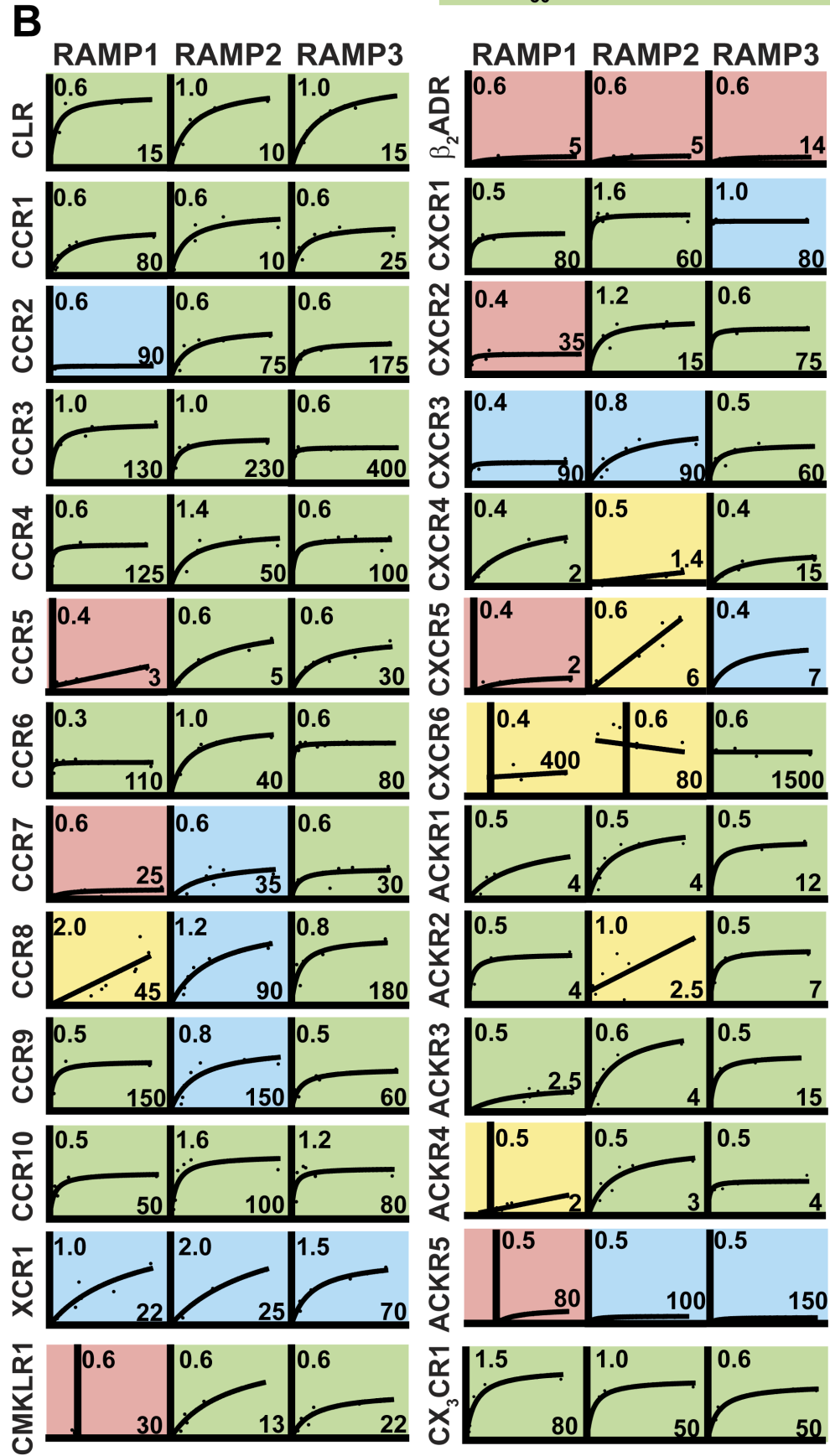
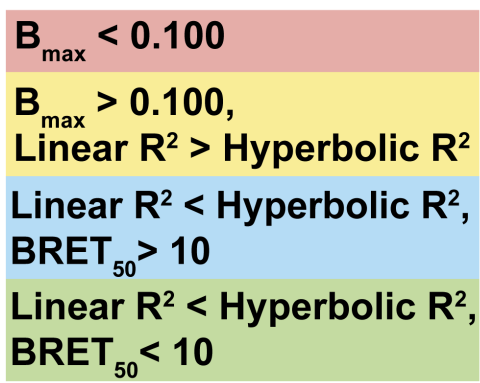
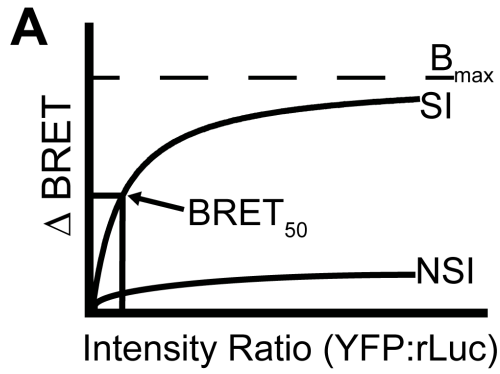
represented by the rightward shift in the EC_{50} from $0.52 \text{ nM} \pm \log EC_{50}=0.05$ to $1.3 \text{ nM} \pm \log EC_{50}=0.08$ (Hill slope for +GLP2R = 0.86 ± 0.08 , Hill slope for +ACKR3 = 0.50 ± 0.05) For both A and B, curves and statistical significance were determined by nonlinear regression with a comparison of fits (F-test), $n=6$ in duplicate. (C) Immunofluorescence confocal microscopy shows ACKR3: RAMP3 colocalized at the plasma membrane. HEK293T cells were either not treated with ligand and fixed, treated with AM for 1 h and fixed, or treated with AM for 1 h washed/ allowed to recover for 4 h, and fixed. After ligand stimulation, ACKR3 and RAMP3 internalized and showed colocalization with NSF intracellularly. ACKR3 in the presence of RAMP3 and NSF (left column) resulted in the ACKR3: RAMP3 complex localizing to the plasma membrane after the four hour recovery phase. ACKR3 in the absence of NSF (center column) or RAMP3 (right column) did not recycle to the plasma membrane after removal of ligand and 4 h recovery. Images are representative of 3 independent experiments. Scale bar $10 \mu\text{m}$.

Fig. 4. RAMP3 rescues internalized ACKR3 from Rab7a-positive late endosomes, diverting the receptor to Rab4-positive rapid recycling vesicles resulting in resensitization after AM treatment. (A) HEK293T cells transfected with RFP-Rab4 and ACKR3 \pm RAMP3/NSF were either not treated with AM, treated with 100 nM AM for 1 h and fixed, or treated and allowed to recover for 4 h. After 1 h AM treatment, ACKR3 +RAMP3/NSF are internalized and show colocalization with Rab4 intracellularly (middle row, first column and inset). In the ACKR3 –RAMP3/NSF condition, ACKR3 is internalized but colocalization with Rab4 does not occur (middle row, third column and inset). After a 4 h recovery time post-AM treatment, in the ACKR3 +RAMP3/NSF cells, ACKR3 and RAMP3 show distribution at the plasma membrane of the cell, demonstrating recycling of the receptor complex (bottom row, first column and inset). In the ACKR3 – RAMP3/NSF cells, after the 4 h recovery, ACKR3 is not present at the plasma membrane and the receptor remained intracellular (bottom row, third column and inset). (B) Conversely, HEK293T cells transfected with GFP-Rab7a and ACKR3 \pm RAMP3/NSF were treated with AM as

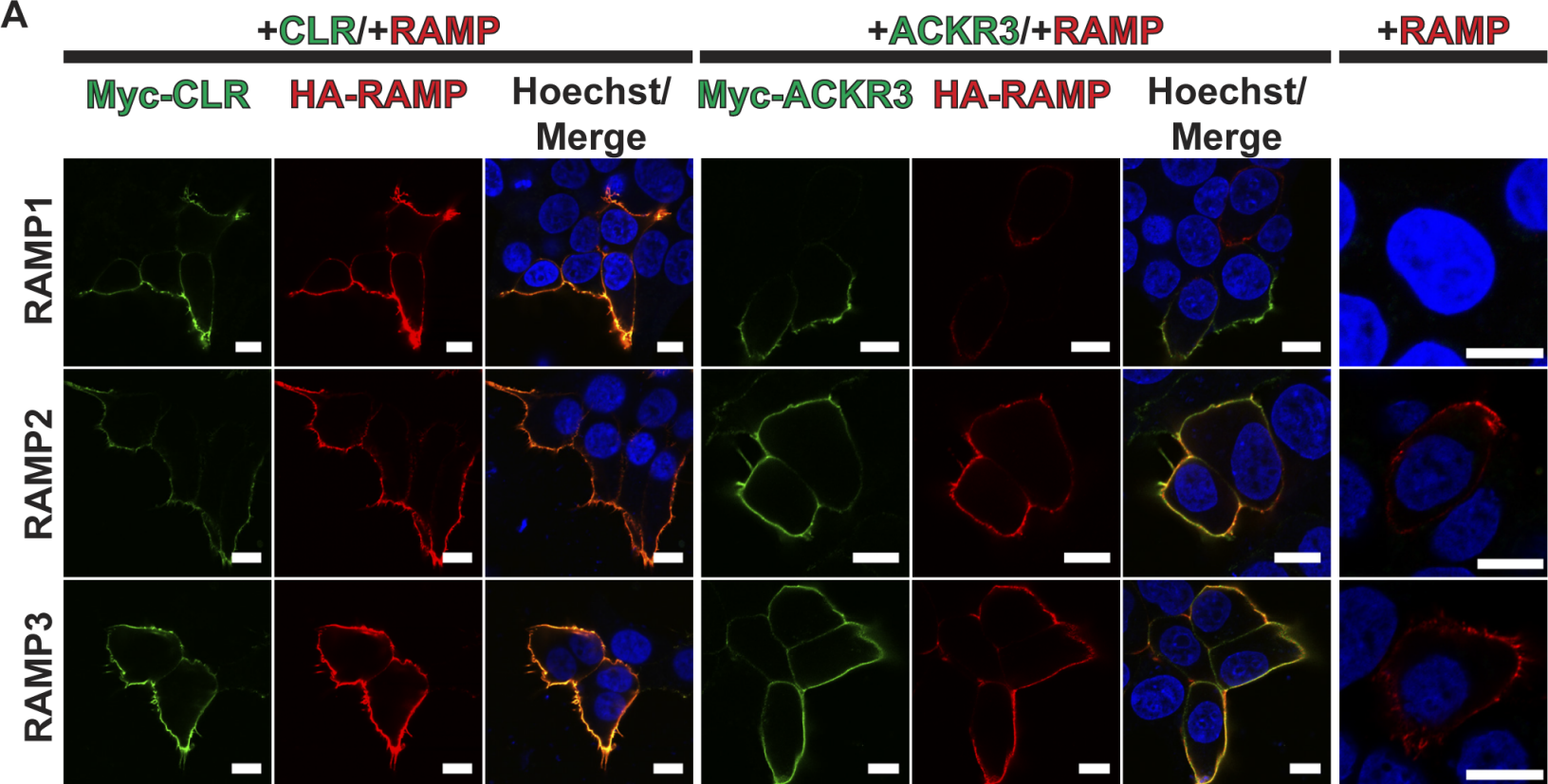
stated above. After 1 h AM treatment, ACKR3 +RAMP3/NSF are internalized and show limited/no colocalization with Rab7a intracellularly (middle row, first column and inset). However, in the ACKR3 –RAMP3/NSF condition, ACKR3 is internalized and shows robust localization in the lumen of Rab7a-positive vesicles (middle row, third column and inset). After a 4 h recovery time post-AM treatment, in the ACKR3 +RAMP3/NSF cells, ACKR3 and RAMP3 show distribution at the plasma membrane of the cell, demonstrating recycling of the receptor complex (bottom row, first column and inset). In the ACKR3 –RAMP3/NSF cells, after the 4 h recovery, ACKR3 is not present at the plasma membrane but is detected in the lumen of Rab7a-late endosomes (bottom row, third column and inset). Images are representative of three independent experiments. Scale bar 10 μ m.

Fig. 5. Vascular development is disrupted upon genetic deletion of ACKR3 or RAMP3 *in vivo* through a RAMP3-mediated rapid recycling mechanism. (A-C) Representative images of whole mount immunofluorescence staining of postnatal day 3 retinal vasculature using isolectin B4 in control, AM over-expressing (*Adm^{hi/hi}*), ACKR3 heterozygous (*Ackr3^{+/-}*), ACKR3 knockout (*Ackr3^{-/-}*), and RAMP3 knockout (*Ramp3^{-/-}*) mice. Statistics were evaluated using n=3-7 mice. Scale Bars, 200 μ M. (D-F) Analysis and quantification of the retinal tip cells detected at the vascular periphery in control and gene targeted mice. Colored dots represent quantitation from different retinal quadrants of individual animals. Statistical significance was determined by an unpaired, 2-tailed t-test with an n between 3-7 mice, as indicated in the figure. Error bars represent SEM of the means. (G) Cartoon depicting gradient-guided migration of vascular endothelial tip cells in response to normal chemotactic gradients (top) established by ACKR3/RAMP3 (yellow/green) and abnormal gradients (bottom) in the absence of ACKR3/RAMP3 ligand scavenging. (J) Model of RAMP3-mediated endosomal sorting of ACKR3. I. Ligand binding of ACKR3 leads to endocytosis of receptor. II. ACKR3 is internalized to early endosomes, where it is colocalized with RAMP3 and NSF. III. The PDZ binding motifs of RAMP3 and NSF are required

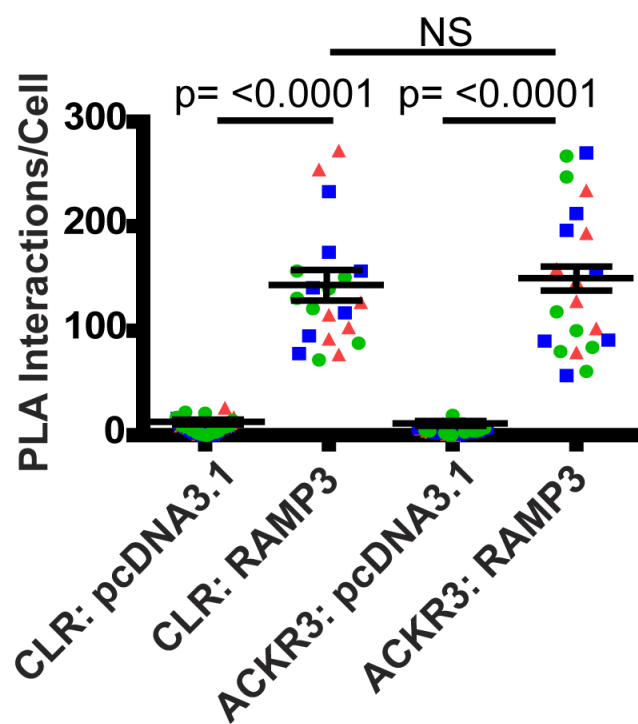
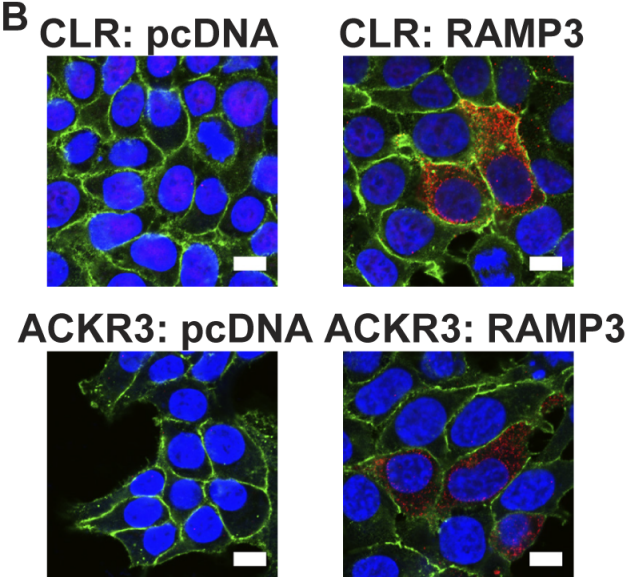
for the Rab4-positive rapid recycling endosome-dependent and RAMP3-facilitated recycling of internalized ACKR3 to the cell surface via a putative interaction with a PDZ domain containing protein. In the absence of RAMP3, ACKR3 is localized to Rab7a-positive late endosomes which controls the trafficking between late endosomes and lysosomes. IV. ACKR3 scavenging is enabled by the rapid resensitization of ACKR3 to the cell surface by RAMP3.



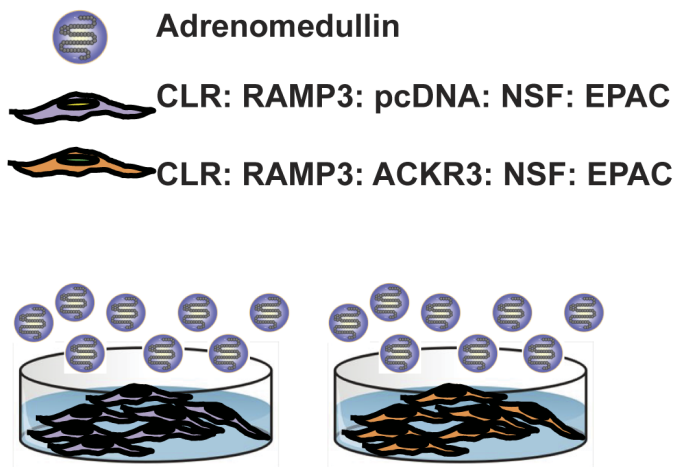
A



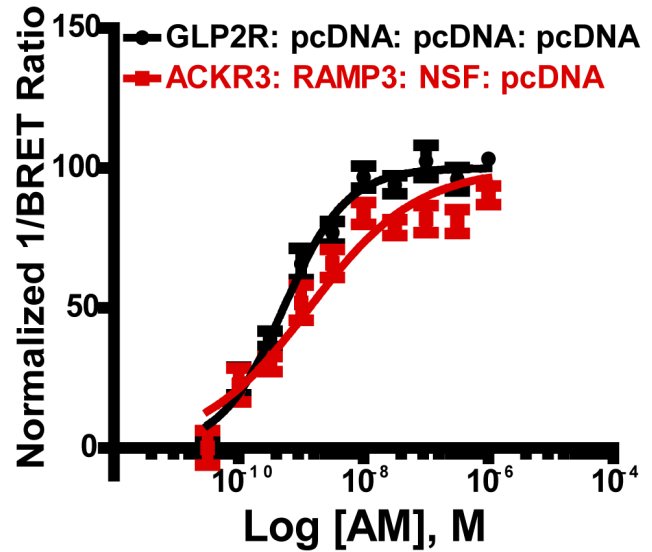
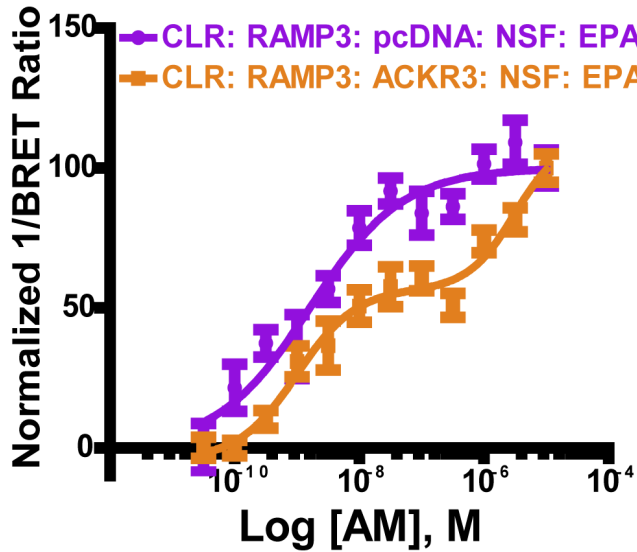
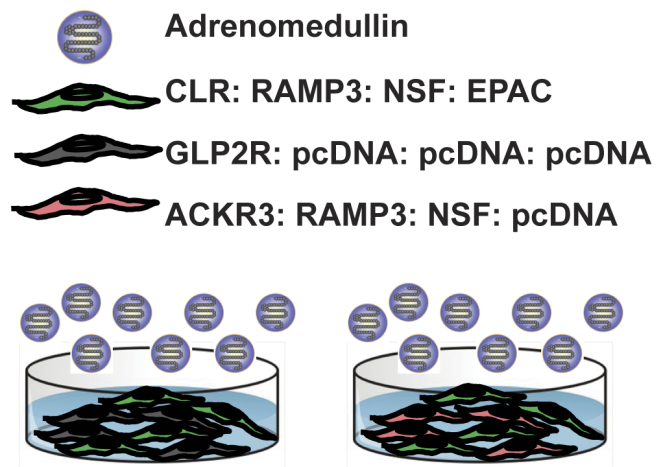
B



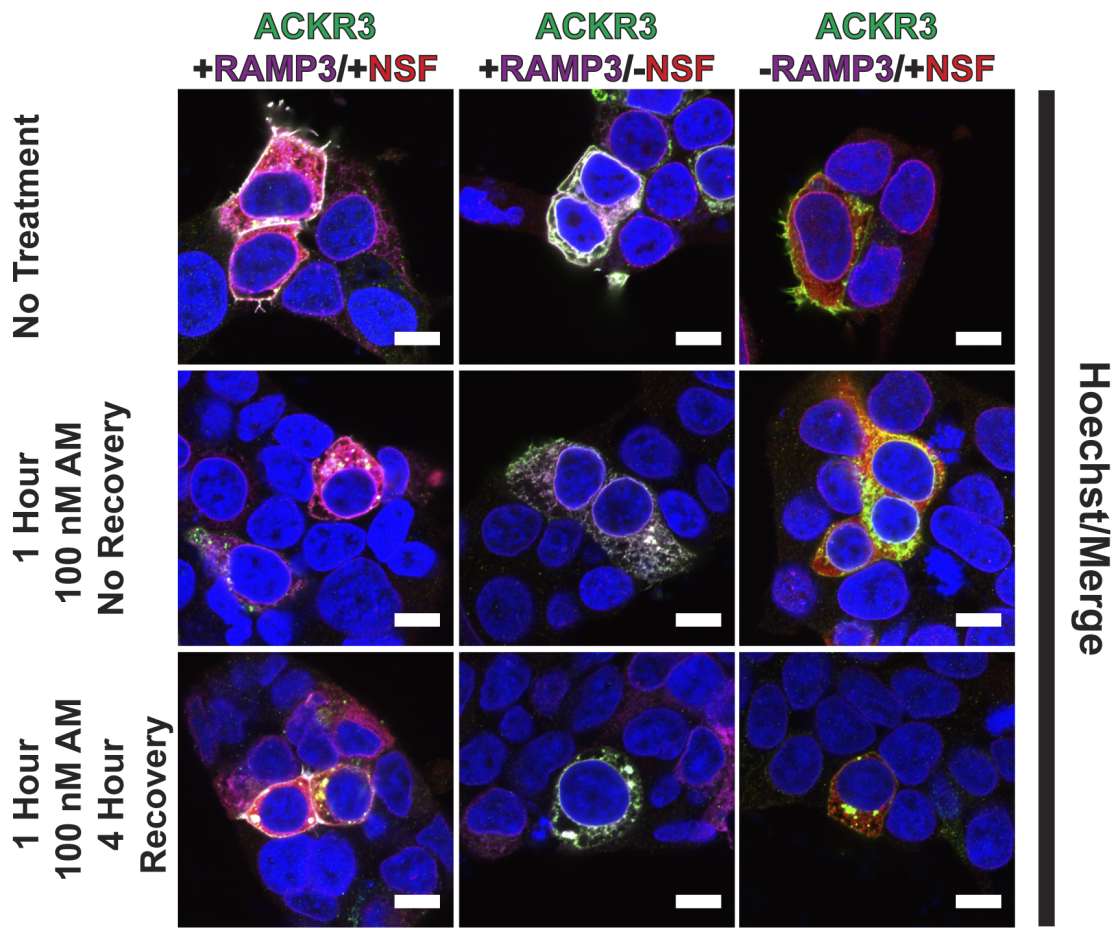
A

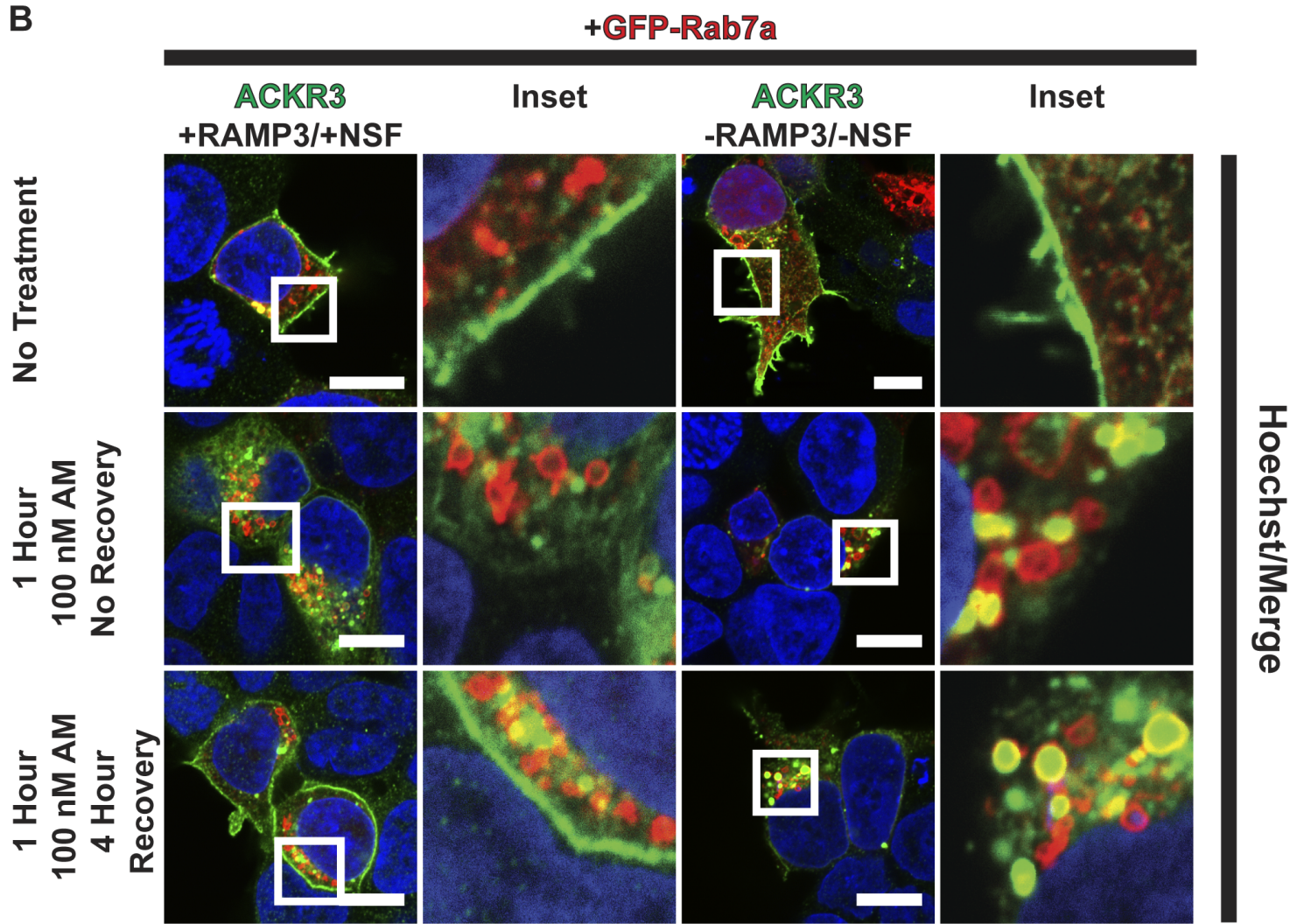
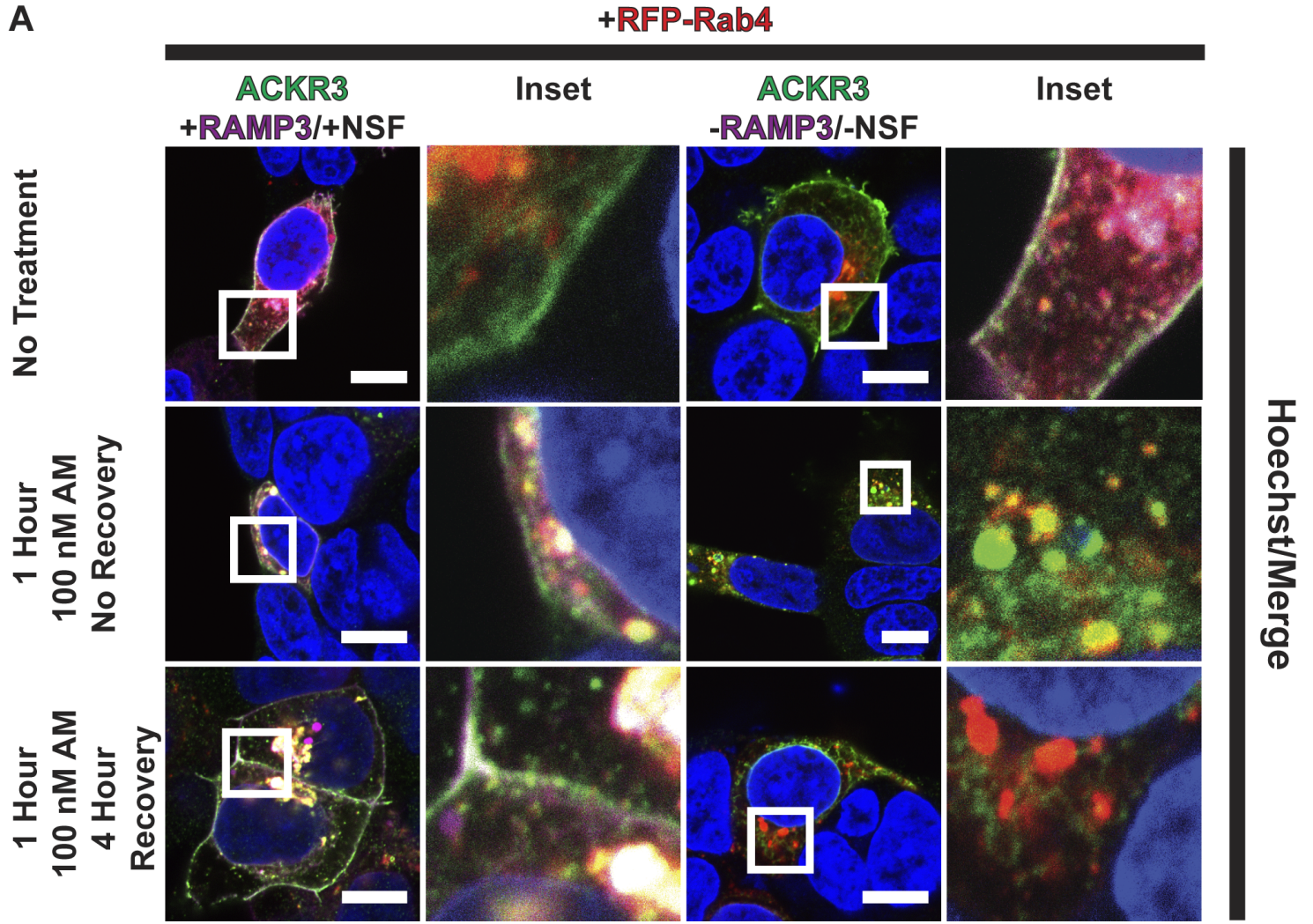


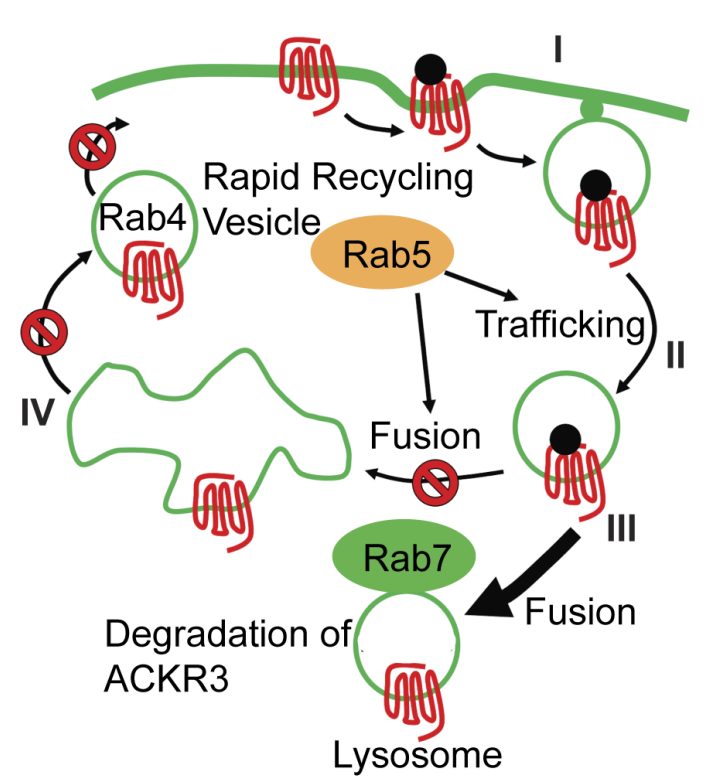
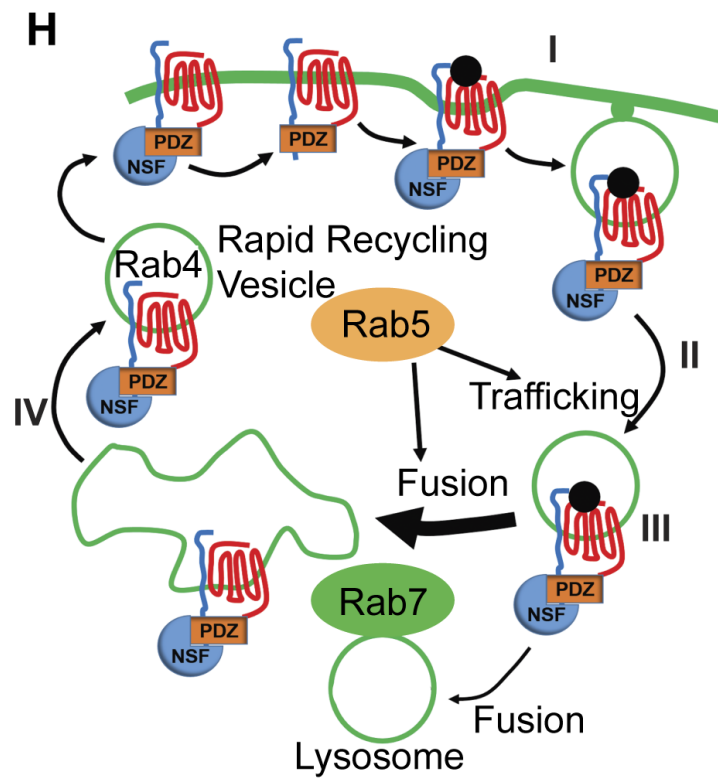
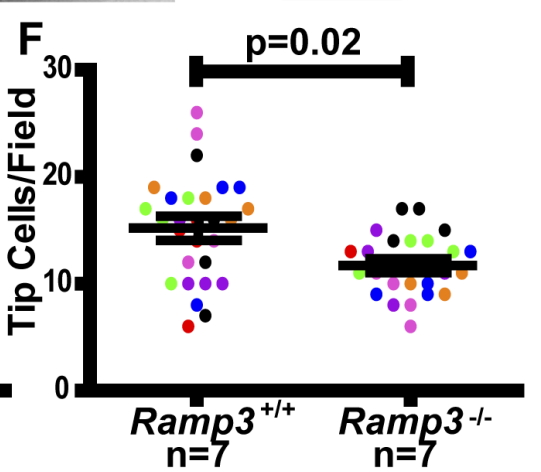
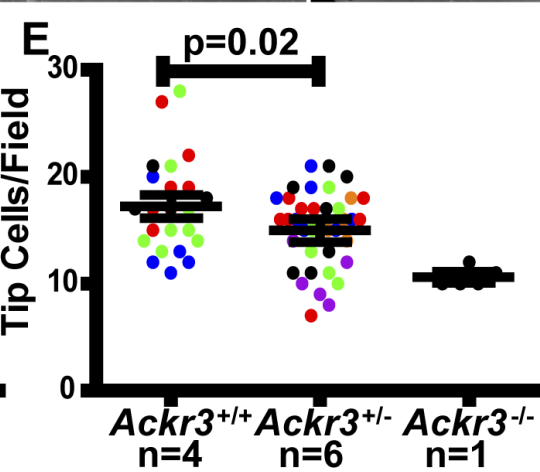
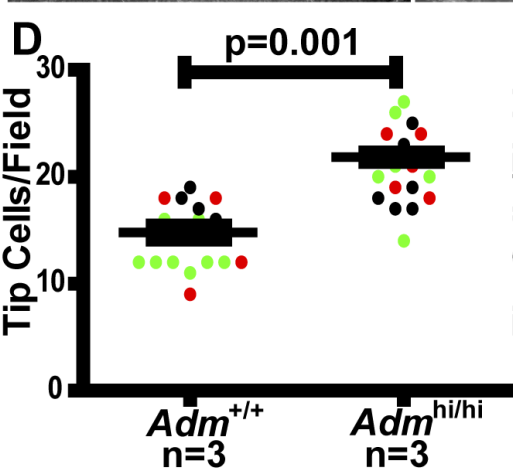
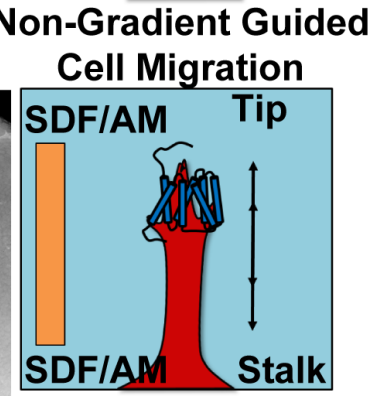
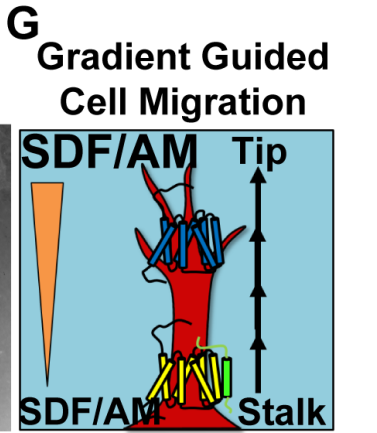
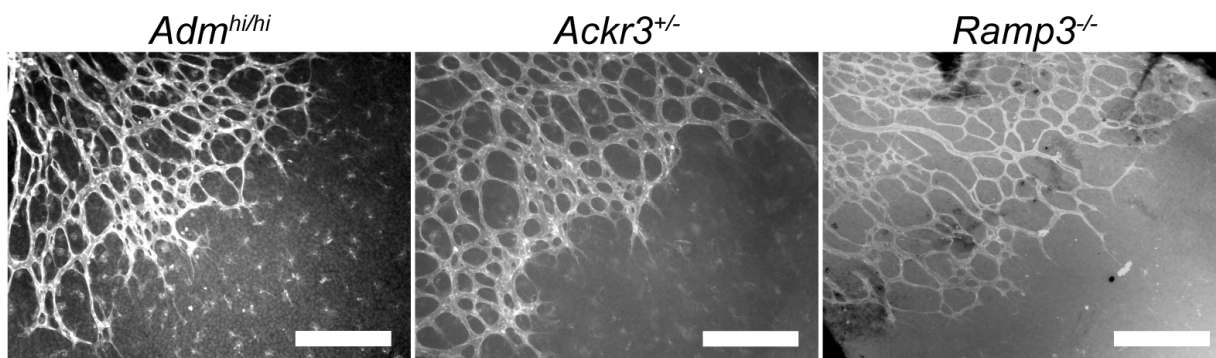
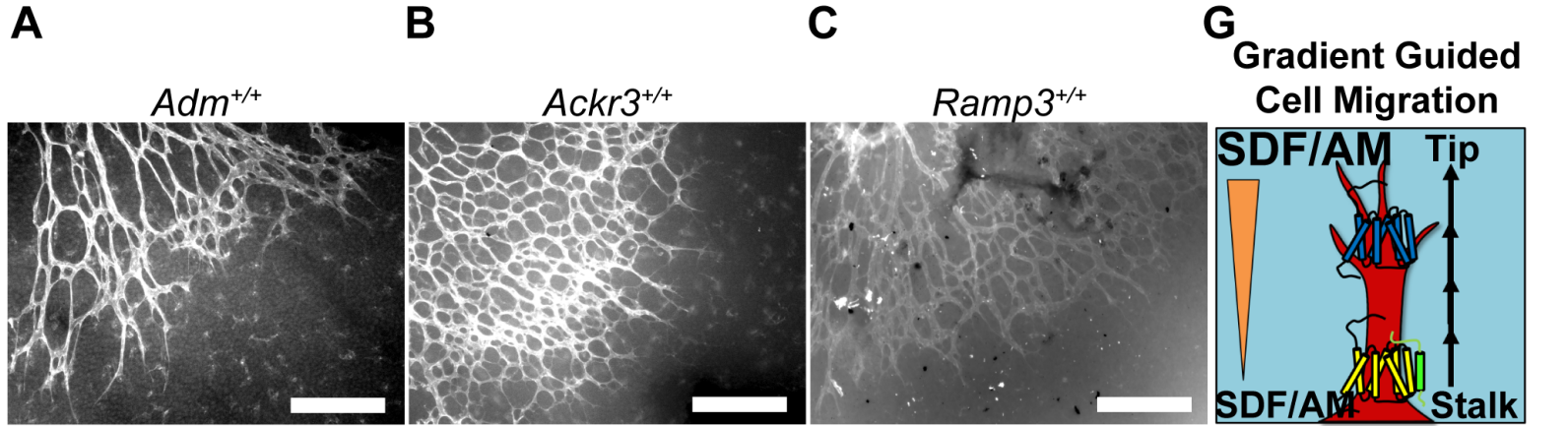
B



C







SI Appendix:

Supplementary Materials and Methods

Generation of expression plasmids

Chemokine receptor cDNA was either purchased from cDNA.org (Bloomsburg University, PA) or a gift from Dr. Sudar Rajagopal (ACKRs 1/2/4/5). All receptors were ligated into a CD33/Myc/rLuc backbone to generate the CD33/Myc/GPCR/rLuc. RAMP-YFP expression plasmids were generated by cloning into the eYFP-N1 expression vector. All cloning results were confirmed by Sanger sequencing (Eton Biosciences, San Diego, CA).

Cell culture and transfection

Human embryonic kidney 293T (HEK293T) cells were maintained in Dulbecco's modified Eagle's medium (DMEM) (Gibco) supplemented with 10% (v/v) fetal bovine serum (Sigma Aldrich), 10 mM HEPES (Corning), 750 μ L gentamicin (Gibco) at 37°C in a humidified atmosphere at 5% CO₂. Transient transfections were performed using lipofectamine 2000 and calcium phosphate where indicated.

COS-7 cells were maintained in DMEM/F12 GlutaMAX™ (Gibco) supplemented with 10% (v/v) heat inactivated fetal bovine serum (Sigma Aldrich) and 1% (v/v) antibiotic antimycotic (Sigma Aldrich) at 37°C in a humidified atmosphere at 5% CO₂. For transient transfections, COS-7 cells were transfected using polyethyleneimine (PEI, 25 KDa, Polyscience Inc., 1 mg/mL) using a 1:3 (w:v) DNA:PEI ratio.

Bioluminescence Resonance Energy Transfer (BRET) measurements

HEK293T cells were seeded at 65,000 cells per well. The next day, the media was changed to 50 μ L optimem and incubated for 2 hours at 37°C. For titration experiments, constant concentration of GPCR-rLuc was used with increasing amount RAMP-YFP from serial dilutions.

In brief, GPCR-rLuc and RAMP-YFP expression vectors were mixed in opti-mem with lipofectamine and incubated for 15 min. Then, the DNA/lipofectamine/opti-mem mixture was added to corresponding wells of the 96-well plate. The next day media was replaced by 90 μ L phosphate-buffer saline containing calcium and magnesium. The assay was started by adding 10 μ L of cell-permeant substrate specific for *R. reniformis* luciferase, coelenterazine *h* (Promega, Madison, WI). The plate was read 10 min after addition of coelenterazine *h* and BRET readings were collected using a Mithras LB940 instrument (Berthold Technologies, Bad Wildbad, Germany) with MicroWin 2000 software (Berthold Technologies USA, Oak Ridge, TN). The acceptor/donor ratio was calculated and the curve was fitted using nonlinear regression and one-site binding with GraphPad Prism.

Flow cytometry

Cos7 cells were seeded in 24 well plates and cultured for 24 hours. Cells were transfected using a mixture of PEI and DNA, diluted in un-supplemented DMEM/F12 GlutaMAX™ to a total volume of 25 μ L and incubated at room temperature for 10 min. For the initial screen, cells were transfected with a total of 0.5 μ g DNA (1:1 ratio of RAMP: receptor/pcDNA3.1-zeo). For RAMP titration experiments, a constant concentration of GPCR (0.2 μ g) was used with increasing amounts of FLAG-RAMP. Forty-eight hours later cells were trypsinised and washed with PBS prior to counting. 200,000 cells were washed three times in FACS buffer (PBS supplemented with 1% BSA and 0.03% sodium azide) before re-suspending in 50 μ L FACS buffer containing either allophycocyanin (APC)-conjugated anti-FLAG monoclonal antibody (BioLegend, diluted 1:80 in FACS buffer) or APC-conjugated anti-HA monoclonal antibody (Colombia Biosciences, diluted 1:40 in FACS buffer), where appropriate and incubated for 1 hour in the dark. The cells received a final three washes in FACS buffer and were re-suspended in 50 μ L FACS buffer. To account for dead cells 2.5 μ L propidium iodide was added to each sample. Samples were analyzed using a BD Accuri C6 flow cytometer (BD Biosciences, excitation λ 633 nm and emission λ 660 nm).

The percentage of events with APC intensity above this threshold was calculated for each test condition, with an increase in intensity indicating FLAG-RAMP translocation to the plasma membrane. For each individual experiment, data were normalized to surface expression of FLAG-RAMP3 when cotransfected with HA-CLR or HA-RAMP3 when cotransfected with myc-CLR-GFP, where appropriate, as 100% and empty vector as 0%. All data was analyzed in GraphPad Prism 8. A one-way ANOVA with Dunnett's post-hoc test was performed to determine any significant differences in cell surface expression of RAMPs compared to cells transfected with RAMP alone.

ACKR3 G protein coupling and β -arrestin recruitment assays

To investigate Gas coupling, HEK293T cells were seeded in 10cm² dish and grown over night. The following day, cells were transfected using calcium phosphate with the specific ACKR3 and RAMP combination and the cAMP-sensitive biosensor EPAC at 2.5 μ g, 2.5 μ g, 4 μ g, respectively. The EPAC biosensor has been studied extensively and has been proven to correlate linearly with agonist induced cAMP levels (1). Cells were grown overnight, trypsinized, and seeded at 100k cells/well into poly-D-lysine coated plates in phenol-red free, serum reduced media (MEM + 2%FBS + 1% Penn/Strep + 1%HEPES). The following day, the media was aspirated and 80 μ L of PBS containing calcium and magnesium was added to each well. Then, 10 μ L Coelenterazine h was added to each well and incubated for 10 min in the dark. Finally, compound was added to the plate and read at 30 min.

Next, for Gai/o coupling, HEK293T cells were seeded and transfected following the protocol described above. After transfected cells were seeded in 96-well plates. The following day 80 μ L of PBS containing calcium and magnesium was added to each well. 10 μ L Coelenterazine h was added to each well, and incubated for 10 min in the dark. A half-log dilution series of peptide ligand was generated which also contains forskolin and this was added to each well, for a final concentration of 10 μ M forskolin/well. The plate was incubated and read at 30 min.

Finally, for β -arrestin1/2 recruitment, HEK293T cells were seeded and transfected following the exact same protocol for G α s signaling, with the exception of the transfected DNA. For β -arrestin recruitment, ACKR3-rLuc (1 μ g) and accompanying RAMP (1 μ g) are transfected with β -arrestin-1-YFP (5 μ g) or β -arrestin-2-YFP (5 μ g) and a GRK (4 μ g). Cells were seeded into a 96-well plate, the next day the media was removed and 80 μ L of PBS was added to each well. 10 μ L Coelenterazine h was added to each well, and incubated for 10 min in the dark. Finally, compound was added to the plate and read at 30 min. Data was analyzed with a non-linear curve fit with a variable slope for either log(agonist) or log(antagonist).

Live cell immunofluorescence confocal microscopy

HEK293T cells were seeding in poly-D-lysine coated Mattek 35 mm dishes and transfected with -CLR/+RAMP1-3, +CLR/+RAMP1-3, or +ACKR3/+RAMP1-3. The next day, cells were washed and incubated in staining media (SM= MEM, +L-Glutamine, +1% HEPES) containing primary antibodies (rabbit anti-Myc at 1:500 and goat anti-HA at 1:250) on ice for 45 min. Staining was stopped by washing the cells with cold PBS 2x and the cells were fixed with 4% paraformaldehyde for 30 min at room temperature. Samples were blocked for 2 hours with 4% BSA in PBS. Appropriate secondary antibodies were applied for 2 hours at room temperature (donkey anti-rabbit Cy2 at 1:200 and donkey anti-goat Cy3 at 1:400). MatTek plates were washed 2x with room temperature PBS and stained for the nucleus with Hoechst at 1:1000 for 10 min. Cells were visualized on a Zeiss 880 confocal laser scanning microscope (UNC Hooker Imaging Core). All images were analyzed in FIJI(2).

In situ proximity ligation assay (PLA)

PLA was performed using a Duolink Fluorescence kit (Sigma Aldrich) according to manufacturer's instructions. HEK293T cells were seeded into 35 mm MatTek plates #P35G-0-10-C (MatTek Corporation, Ashland, MA). The following day, cells were transfected with 250 ng of

CD33/Myc/ACKR3 and Native Signal Sequence/3xHA/RAMP or pcDNA3.1 with calcium-phosphate transfection mixture (3). The next day, the cells were washed with 1xPBS, fixed, permeabilized, and incubated with primary antibodies (Rabbit anti-Myc at 1:500 and Goat anti-HA at 1:250) followed by incubation with anti-rabbit minus and anti-goat plus PLA probes, and finally with ligation and amplification mixtures. PLA reactions were further stained with β -catenin-FITC (Sigma) and Hoechst to mark the cell walls and nucleus, respectively. Images were observed under Zeiss 880 confocal laser scanning microscope under 63x, oil emersion objective. A field of confluent cells was imaged and all cells with PLA signal were selected for counting. Images were processed with FIJI, and red spots were counted using Blob Finder software(4).

Scavenger assay

HEK293T cells were transiently transfected with the EPAC sensor and either CLR: RAMP3: pcDNA: NSF or CLR: RAMP3: ACKR3: NSF. The following day, cells were seeding into 96-well plates in low serum MEM. Twenty-four hours later the media was aspirated and 80 μ l of PBS containing calcium and magnesium was added to each well followed by addition of 10 μ l coelenterazine solution (final concentration, 5 μ M). After 10-min incubation in the dark, a 10x concentrated solution of a half-log dilution series of AM in PBS was added to each well and read on a Berthold Mithras LB940 instrument and using MicroWin 2000 software (Berthold Technologies).

In the second experiment, HEK293T cells were transiently transfected with the EPAC sensor and CLR: RAMP3: pcDNA, generating the reporter cells. HEK293T cells were transfected with either ACKR3: RAMP3: NSF: pcDNA or GLP2R: pcDNA: pcDNA: pcDNA. The following day, the cells were seeding into 96-well plates as a 50/50 mixture (50k CLR reporter cells with 50k ACKR3 cells or 50k CLR reporter cells with 50k GLP2R cells) in low serum MEM. Twenty-four hours later the media was aspirated and 80 μ l of PBS containing calcium and magnesium was added to each well followed by addition of 10 μ l of a 50 μ M coelenterazine solution (final

concentration, 5 μ M). After 10-min incubation in the dark, a 10 \times concentrated solution of a half-log dilution series of AM in PBS was added to each well and the plate was then read as previously described above. Curves and statistical significance were determined by nonlinear regression with a comparison of fits (F-test) in GraphPad Prism.

Internalization, resensitization, and trafficking assays

HEK293T cells were transfected with ACKR3 \pm RAMP3 and \pm NSF or CLR \pm RAMP3 and \pm NSF. Twenty-four hours post-transfection cells were treated with or without 100 nM AM for 1 h and fixed or allowed to recover. After agonist exposure, for receptor resensitization, cells were washed and incubated for 4 h in complete DMEM containing 5 μ g/ml cycloheximide. Cells were washed 3x with PBS and fixed with 4% paraformaldehyde for 30 min at room temperature. Samples were permeabilized with 0.1% v/v Triton X-100 in PBS for 15 min and blocked overnight in PBS + 4% BSA. Samples were incubated in primary antibody in blocking buffer for 2 h at room temperature (mouse anti-NSF at 1:250, rabbit anti-Myc at 1:500 and goat anti-HA at 1:250). Appropriate secondary antibodies were applied for 2 h at room temperature (donkey anti-mouse Cy3 at 1:300, donkey anti-goat Cy5 at 1:300, and donkey anti-rabbit Cy2 at 1:300).

To track ACKR3 recycling in endosomal compartments, HEK293T cells were cultured on poly-d-lysine coated 35 mm MatTek plates and transfected with ACKR3 +RFP-Rab4 and \pm RAMP3/NSF or ACKR3 +GFP-Rab7a and \pm RAMP3/NSF. For recycling experiments using the RAMP3 Δ PDZ protein, the same dosing paradigm was followed except cells were transfected with ACKR3 +RFP-Rab4 and +RAMP3 Δ PDZ/NSF, ACKR3 +GFP-Rab7a and +RAMP3 Δ PDZ/NSF or ACKR3 +RFP-Rab11 and +RAMP3 Δ PDZ/NSF. Cells were treated with 100 nM AM or 15 nM CXCL12, fixed and permeabilized. Fixed cells were incubated with primary antibody in blocking buffer for 2 h at room temperature (rabbit anti-Myc at 1:500 and goat anti-HA at 1:250). Appropriate secondary antibodies were applied for 2 h at room temperature (donkey anti-goat Cy5 at 1:300, and donkey anti-rabbit Cy2 or Cy3 depending on the Rab protein at 1:300). All cells

were visualized with a Zeiss 880 confocal laser scanning microscope under 63x, oil emersion objective. All images were processed with FIJI.

Retina staining and whole-mount imaging

P3 retinas were isolated, flat-mounted, and stained with BS-I isolectin B4 FITC conjugated antibody (Sigma, L2895) in Immunomix blocking solution overnight at 4°C. Whole-mount fluorescent-stained retina images were captured using a Leica M205FA fluorescent stereoscope with QImaging Micropublisher 5.0 RTV color CCD camera. Statistical significance was determined by an unpaired t test, with *P* values of less than 0.05 considered significant.

1. Breton B, *et al.* (2010) Multiplexing of multicolor bioluminescence resonance energy transfer. *Biophysical journal* 99(12):4037-4046.
2. Schindelin J, *et al.* (2012) Fiji: an open-source platform for biological-image analysis. *Nature methods* 9(7):676-682.
3. Kingston RE, Chen CA, & Okayama H (2003) Calcium phosphate transfection. *Current protocols in cell biology / editorial board, Juan S. Bonifacino ... [et al.]* Chapter 20:Unit 20 23.
4. Allalou A & Wahlby C (2009) BlobFinder, a tool for fluorescence microscopy image cytometry. *Computer methods and programs in biomedicine* 94(1):58-65.

Supplementary Table and Figures

Table S1

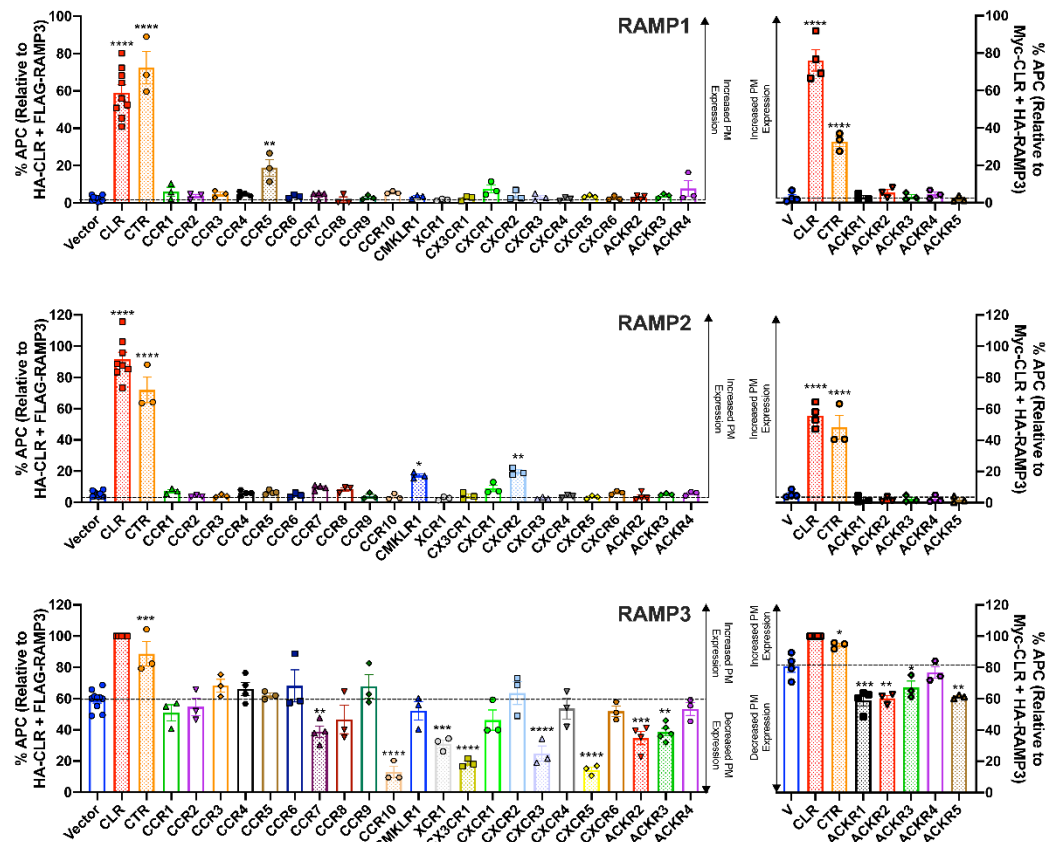
IUPHAR receptor name	N	Receptor Expression (RLU) +/- SEM	BRET50 (RAMP1)	Bmax (RAMP1)	BRET50 (RAMP2)	Bmax (RAMP2)	BRET50 (RAMP3)	Bmax (RAMP3)
CLR	3	401536 +/- 58253	1.547 ± 0.932	0.449 ± 0.030	1.803 ± 0.313	0.872 ± 0.163	1.875 ± 1.335	1.618 ± 0.533
β ₂ ADR	3	359986 +/- 34576	—	<0.1*	—	<0.1*	—	<0.1*
CCR1	4	117146 +/- 10608	9.8 ± 1.930	0.247 ± 0.016	5.794 ± 2.330	0.490 ± 0.034	5.962 ± 2.275	0.234 ± 0.009
CCR2	4	169327 +/- 16338	19.5 ± 19.25	0.123 ± 0.036	4.718 ± 2.638	0.279 ± 0.034	5.176 ± 2.067	0.195 ± 0.029
CCR3	4	84896 +/- 6359	5.751 ± 1.837	0.655 ± 0.050	5.133 ± 2.662	0.475 ± 0.017	1.217 ± 0.691	0.212 ± 0.012
CCR4	3	103687 +/- 6495	3.437 ± 1.607	0.297 ± 0.011	4.384 ± 1.388	0.804 ± 0.043	1.417 ± 0.727	0.280 ± 0.024
CCR5	3	332685 +/- 80312	—	<0.1*	2.185 ± 0.383	0.500 ± 0.047	3.256 ± 2.736	0.205 ± 0.100
CCR6	3	156276 +/- 17089	2.649 ± 1.132	0.126 ± 0.005	3.907 ± 0.892	0.681 ± 0.051	0.653 ± 0.206	0.332 ± 0.010
CCR7	3	123234 +/- 7719	—	<0.1*	16.62 ± 3.843	0.274 ± 0.007	3.723 ± 1.529	0.225 ± 0.010
CCR8	3	117040 +/- 12702	LF	LF	15.84 ± 8.872	1.042 ± 0.091	6.464 ± 2.784	0.603 ± 0.011
CCR9	3	97589 +/- 11024	2.926 ± 0.622	0.249 ± 0.013	11.97 ± 9.840	0.464 ± 0.061	2.903 ± 0.538	0.233 ± 0.008
CCR10	3	76897 +/- 4952	2.641 ± 0.356	0.326 ± 0.042	6.817 ± 2.407	1.159 ± 0.026	1.233 ± 0.433	0.612 ± 0.033
CMKLR1	3	146240 +/- 13319	—	<0.1*	3.596 ± 1.862	0.432 ± 0.146	6.967 ± 2.611	0.283 ± 0.024
XCR1	3	73409 +/- 8187	41.47 ± 18.41	1.904 ± 0.466	22.77 ± 7.231	2.360 ± 0.277	16.52 ± 2.170	1.228 ± 0.060
CX ₃ CR1	3	202698 +/- 24901	5.285 ± 2.16	0.693 ± 0.262	3.25 ± 1.092	0.469 ± 0.100	5.715 ± 0.649	0.290 ± 0.041
CXCR1	3	60780 +/- 6248	3.314 ± 0.765	0.184 ± 0.016	6.243 ± 2.912	0.452 ± 0.282	12.98 ± 7.305	0.468 ± 0.046
CXCR2	3	208640 +/- 9289	—	<0.1*	3.114 ± 1.487	0.627 ± 0.053	2.675 ± 1.830	0.289 ± 0.023
CXCR3	3	212779 +/- 31503	11.16 ± 9.663	0.118 ± 0.030	15.84 ± 5.409	0.461 ± 0.042	6.758 ± 2.171	0.242 ± 0.013
CXCR4	3	591625 +/- 82342	0.936 ± 0.201	0.375 ± 0.065	LF	LF	2.968 ± 0.214	0.170 ± 0.010
CXCR5	4	317226 +/- 72607	—	<0.1*	LF	LF	17.18 ± 12.32	0.290 ± 0.052
CXCR6	3	103335 +/- 23198	LF	LF	LF	LF	HC	0.284 ± 0.006
ACKR1	3	878280 +/- 81508	0.980 ± 0.426	0.190 ± 0.083	1.001 ± 0.188	0.298 ± 0.058	0.801 ± 0.199	0.233 ± 0.043
ACKR2	3	1163000 +/- 57502	0.886 ± 0.578	0.182 ± 0.052	LF	LF	0.384 ± 0.147	0.237 ± 0.034
ACKR3	4	482451 +/- 87645	1.374 ± 0.385	0.152 ± 0.044	2.333 ± 1.468	0.522 ± 0.069	1.901 ± 1.289	0.275 ± 0.035
ACKR4	3	1152000 +/- 170957	LF	LF	1.316 ± 0.442	0.366 ± 0.032	0.494 ± 0.053	0.164 ± 0.017
ACKR5	3	271324 +/- 9213	—	<0.1*	27.43 ± 17.83	0.104 ± 0.043	135.0 ± 90.89	0.194 ± 0.093

RLU: Relative Fluorescence Units, LF: Linear Fit, HC: Hit Constraint, SEM: Standard Error of the Mean

* Denotes that the maximum measured BRET value was <0.1; "—" indicates no detectable BRET50

Fig. S1

A



B

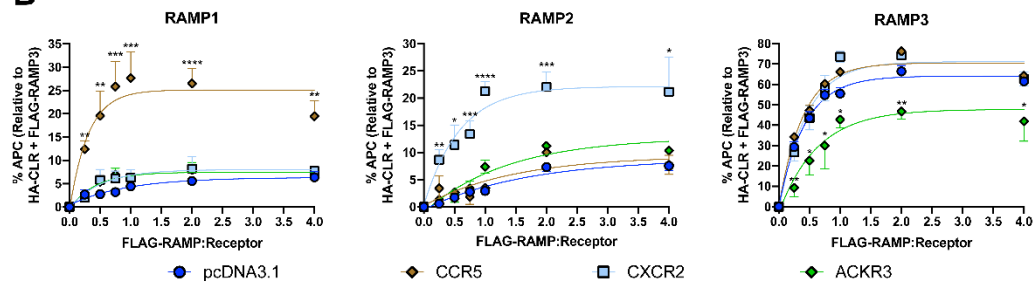


Fig. S1. Fluorescence-activated cell sorting (FACS) analysis of chemokine receptor dependent surface expression of RAMPs. Cos7 cells were cotransfected with GPCR and RAMP at a 1:1 ratio. Plasma membrane expression of RAMPs was determined for each GPCR:RAMP pair by flow cytometry using either an allophycocyanin (APC)-conjugated anti-FLAG monoclonal antibody (left hand panels) or an APC-conjugated anti-HA monoclonal antibody (right hand panels). An increase in APC intensity, relative to RAMP expressed alone, indicated GPCR-dependent promotion of RAMP cell surface expression, whilst a decrease in APC intensity indicated GPCR-dependent attenuation of RAMP cell surface expression. Plasma membrane expression was normalized to RAMP3 when cotransfected with calcitonin receptor-like receptor (CLR) as 100 %. Calcitonin receptor (CTR) is displayed as a positive control for a receptor that does not require RAMPs for plasma membrane expression. (B) Cos7 cells were transfected with a constant amount of CCR5, CXCR2 or ACKR3 and increase amounts of FLAG-RAMPs.

Saturation curves were calculated using one site binding (hyperbola). All values are the mean \pm S.E.M of at least three individual experiments. Data were determined as statistically different (*, $p < 0.05$; **, $p < 0.01$; ***, $p < 0.001$; ****, $p < 0.0001$) compared to RAMP surface expression in the absence of receptor using a one-way ANOVA with Dunnett's post-hoc test.

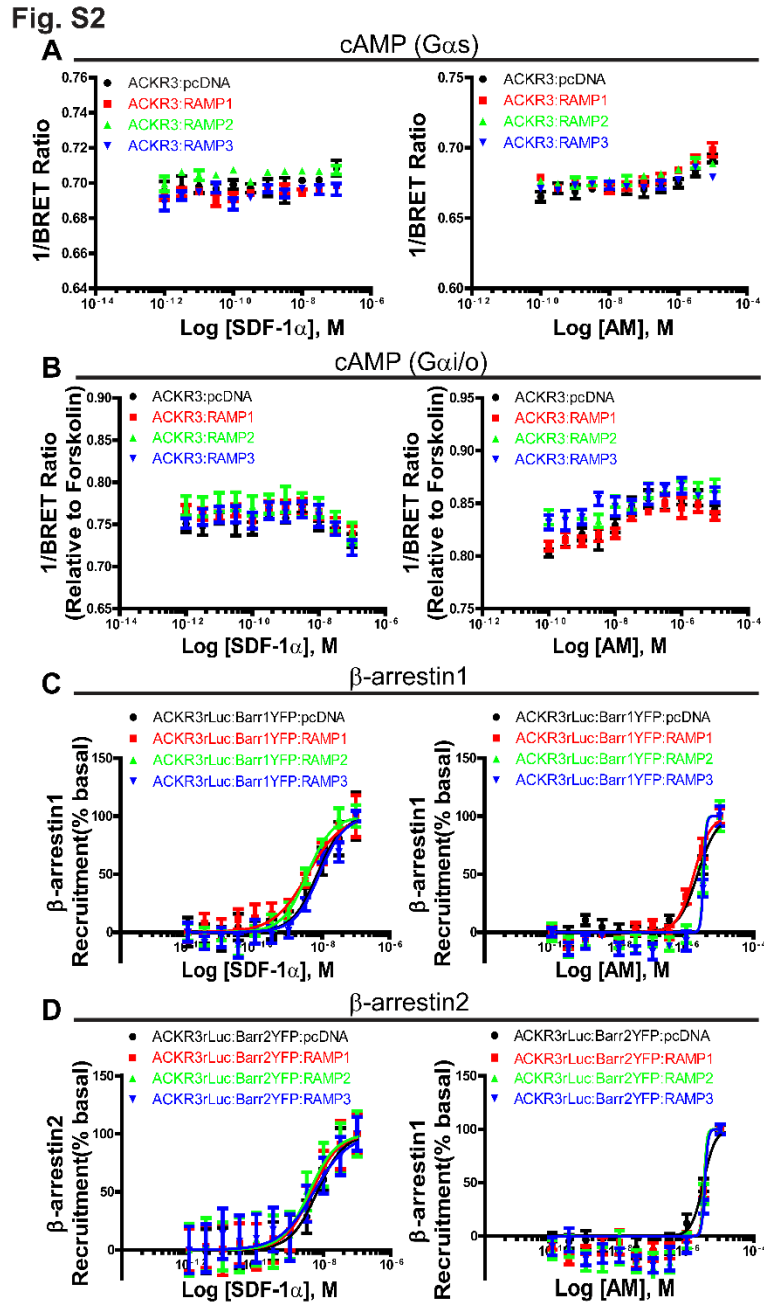


Fig. S2. Systematic analysis of G protein coupling and beta-arrestin recruitment by ACKR3 in the presences and absences of RAMPs with the peptide ligands SDF-1 and AM. (A) $G\alpha_s$ -dependent cAMP production following transient expression of ACKR3 and RAMPs in HEK293T cells was determined utilizing the EPAC biosensor. Upon treatment with either SDF-1 or AM, there was no detectable accumulation of intracellular cAMP. **(B)** $G\alpha_i/o$ -dependent inhibition of

cAMP production was examined through the direct activation of adenylyl cyclase by pretreating ACKR3/RAMP expressing HEK293T cells with forskolin. No Gai/o activity is observed after ligand addition. (C) SDF-1 and AM both recruited β -arrestin1 to ACKR3 independent of RAMP expression, with SDF-1 exhibiting a much higher potency than AM. (D) SDF-1 and AM recruited β -arrestin2 to ACKR3 again independent of RAMPs. Best fit calculated by a nonlinear regression with four parameters and variable slope, \pm S.E.M., $n = 3$ in duplicate. Curves and statistical significance were determined by nonlinear regression with a comparison of fits (F-test).

Fig. S3

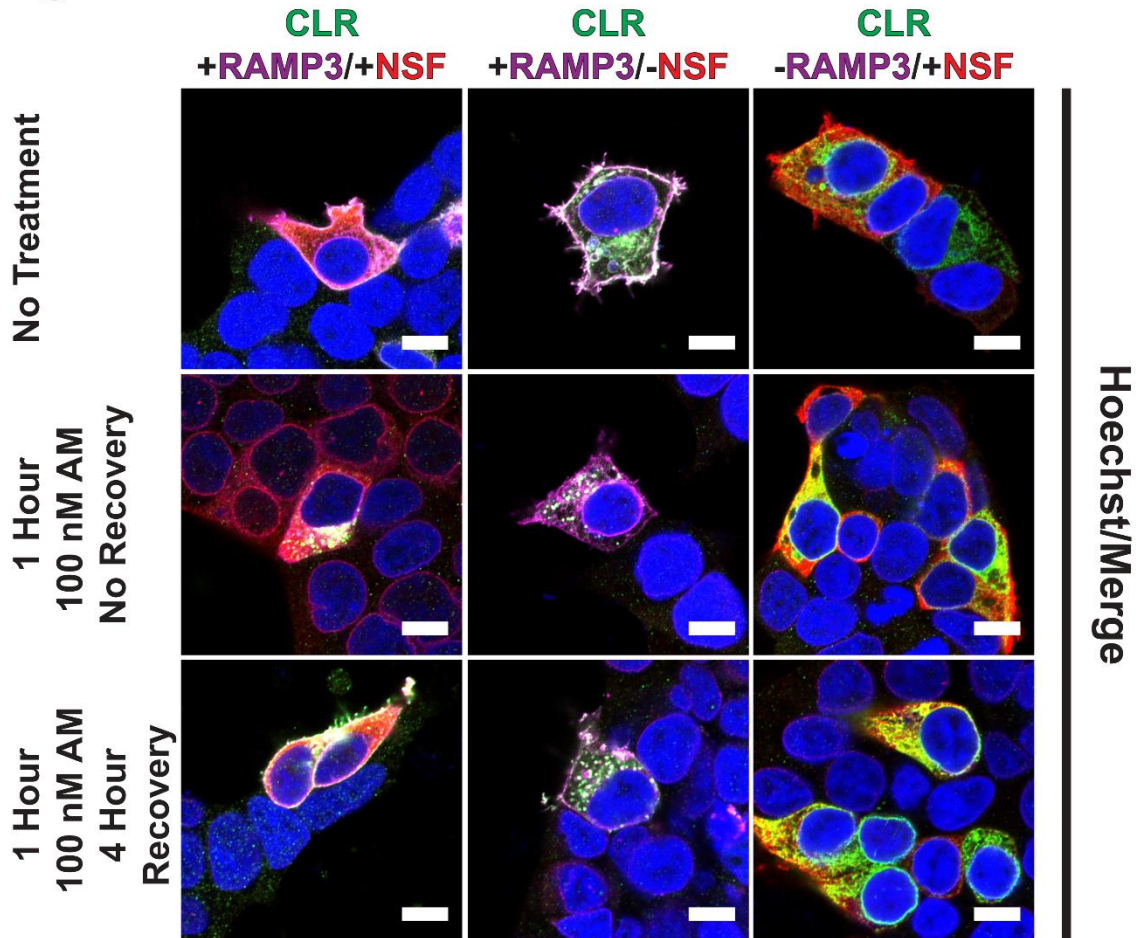


Fig. S3. Localization of CLR, RAMP3, and NSF in HEK293T cells during recycling upon treatment with the peptide ligand AM. Immunofluorescence confocal microscopy shows CLR: RAMP3 colocalized at the plasma membrane. HEK293T cells were either not treated with ligand and fixed, treated with AM for 1 h and fixed, or treated with AM for 1 h washed/ allowed to recover for 4 h, and fixed. After ligand stimulation, CLR and RAMP3 internalized and showed colocalization with NSF intracellularly. Cells that were washed and allowed to recover were incubated in media with 5 μ g/mL cycloheximide to allow receptor recycling. CLR in the presence of RAMP3 and NSF (left column) resulted in the CLR: RAMP3 complex localizing to the plasma membrane after the 4 h recovery phase. CLR in the absence of NSF (center column) or RAMP3 (right column) did not recycle to the plasma membrane after removal of ligand and 4 h recovery. Images are representative of 3 independent experiments. Scale bar 10 μ m.

Fig. S4

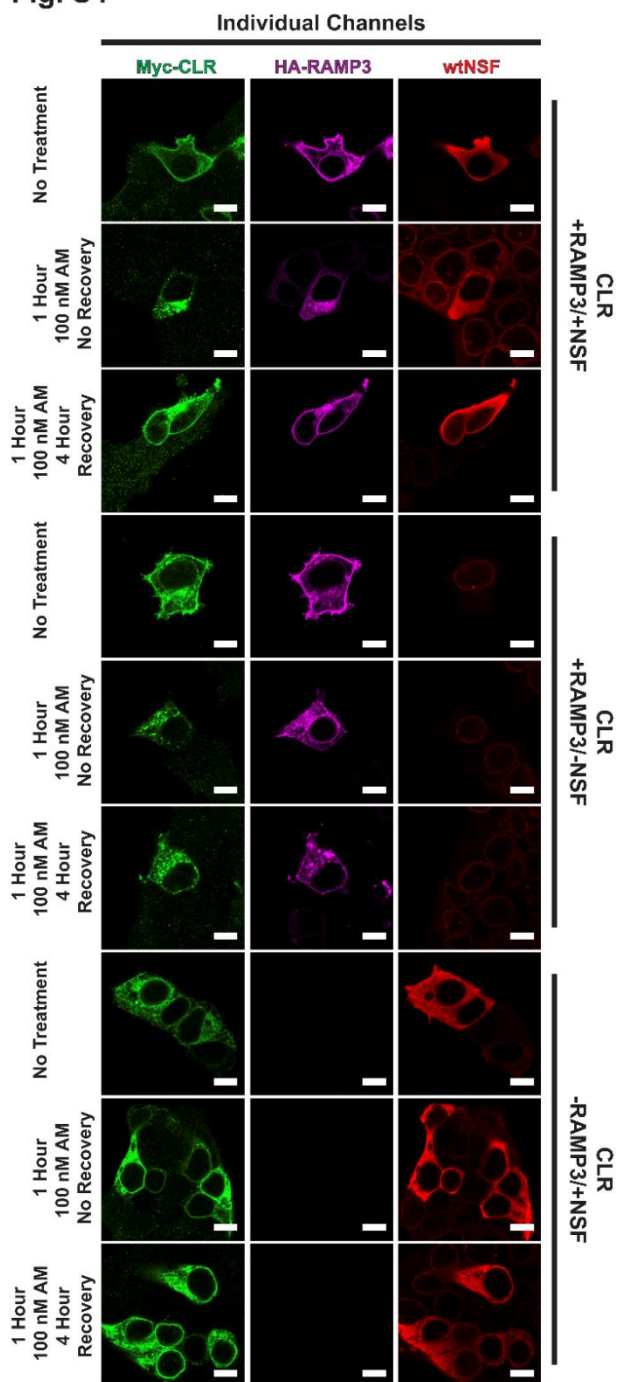


Fig. S4. Individual channels for each protein during recycling in supplemental figure S3. HEK293T cells are transfected with CLR \pm RAMP3 and \pm NSF then cultured overnight. Cells were either not treated with ligand and fixed, treated with AM for 1 h and fixed, or treated with AM for 1 h washed/ allowed to recover for 4 h, and fixed. The first column represents Myc-CLR staining (green), the second column represents HA-RAMP3 staining (magenta), and the third column represents wtNSF staining (red). Treatments and transfection conditions can be found on the left and right of images, respectively. Images are representative of 3 independent experiments. Scale bar 10 μ m.

Fig. S5

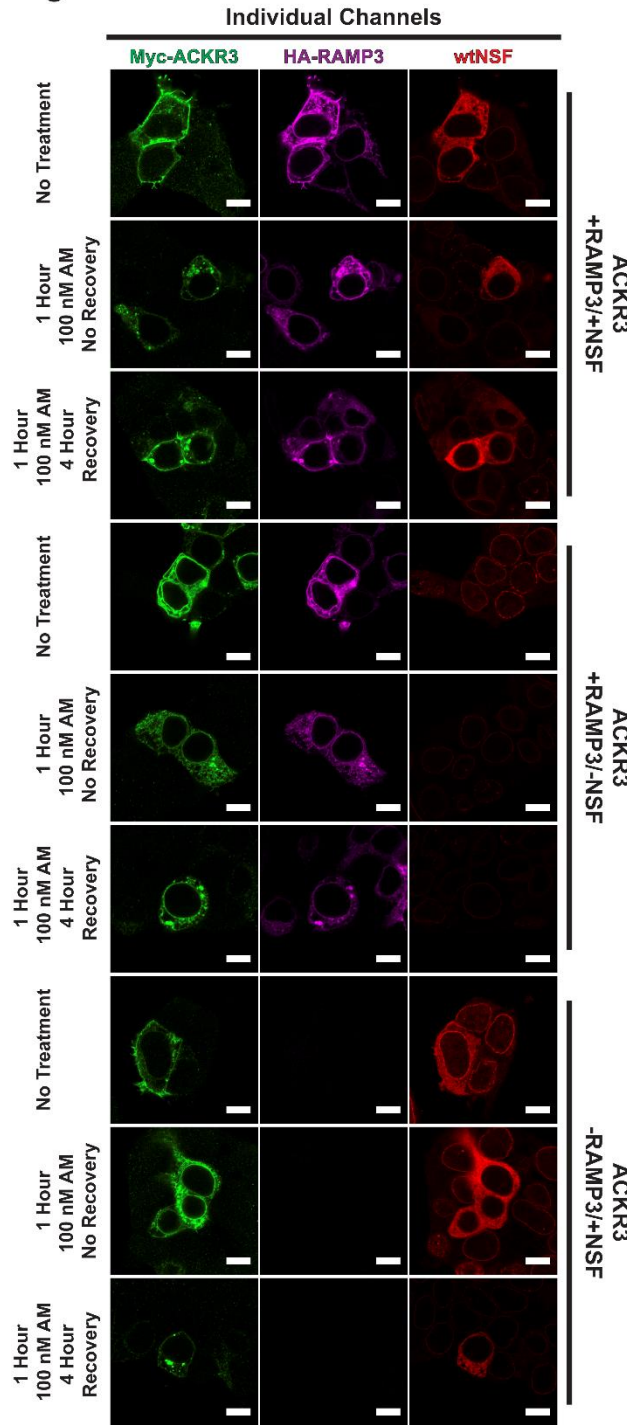


Fig. S5. Individual channels for each protein during recycling in figure 3C. HEK293T cells are transfected with ACKR3 \pm RAMP3 and \pm NSF then cultured overnight. Cells were either not treated with ligand and fixed, treated with AM for 1 h and fixed, or treated with AM for 1 h washed/allowed to recover for 4 h, and fixed. The first column represents Myc-ACKR3 staining (green), the second column represents HA-RAMP3 staining (magenta), and the third column represents wtNSF staining (red). Treatments and transfection conditions can be found on the left and right of images, respectively. Images are representative of 3 independent experiments. Scale bar 10 μ m.

Fig. S6

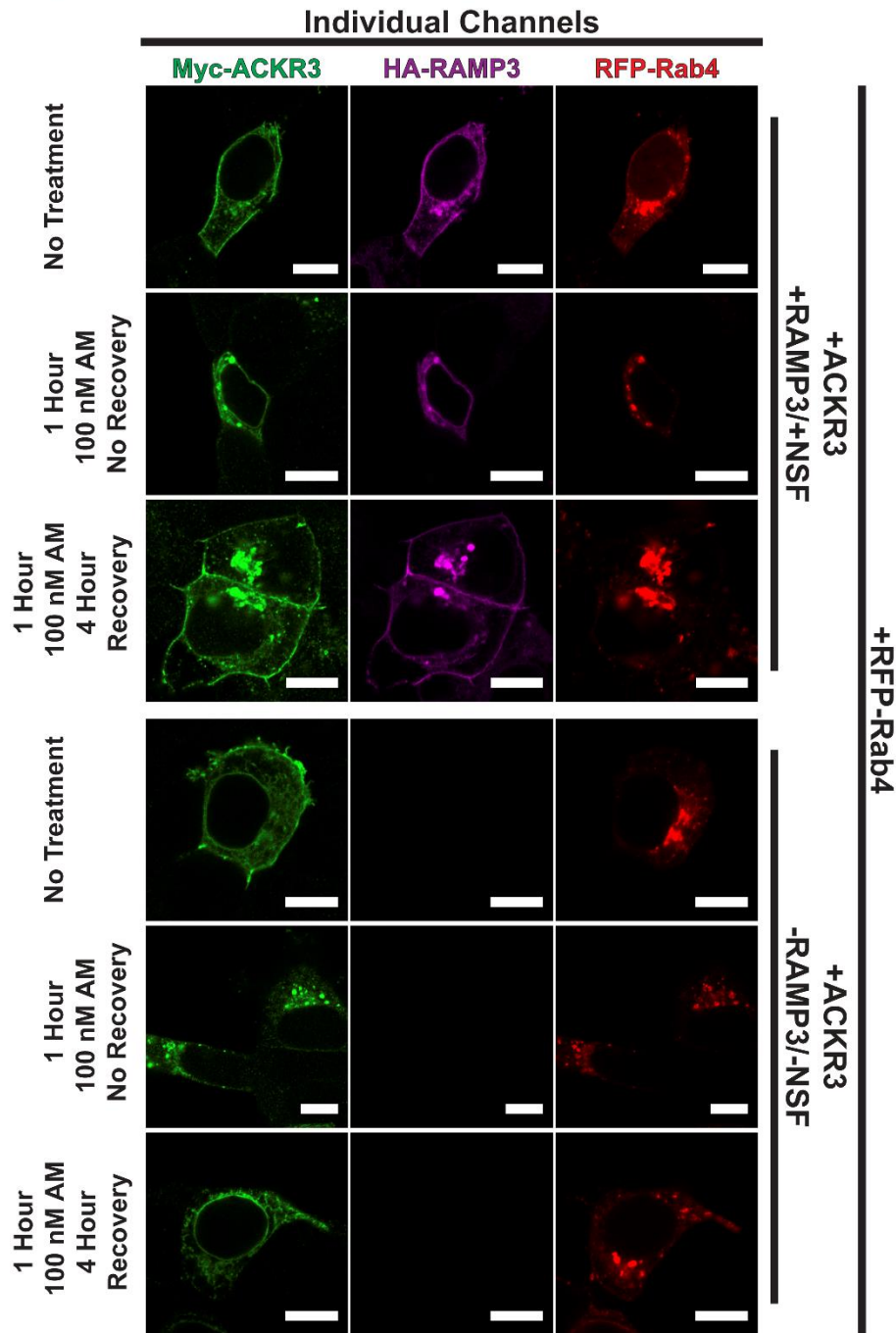


Fig. S6. Individual channels for each protein during ACKR3: RAMP3: Rab4 recycling experiments in figure 4A. HEK293T cells are transfected with ACKR3 \pm RAMP3/NSF and RFP-Rab4 then cultured overnight. Cells were either not treated with ligand and fixed, treated with AM for 1 h and fixed, or treated with AM for 1 h washed/ allowed to recover for 4 h, and fixed. The first column represents Myc-ACKR3 staining (green), the second column represents HA-RAMP3 staining (magenta), and the third column represents RFP-Rab4 expression (red). Treatments and transfection conditions can be found on the left and right of images, respectively. Images are representative of 3 independent experiments. Scale bar 10 μ m.

Fig. S7

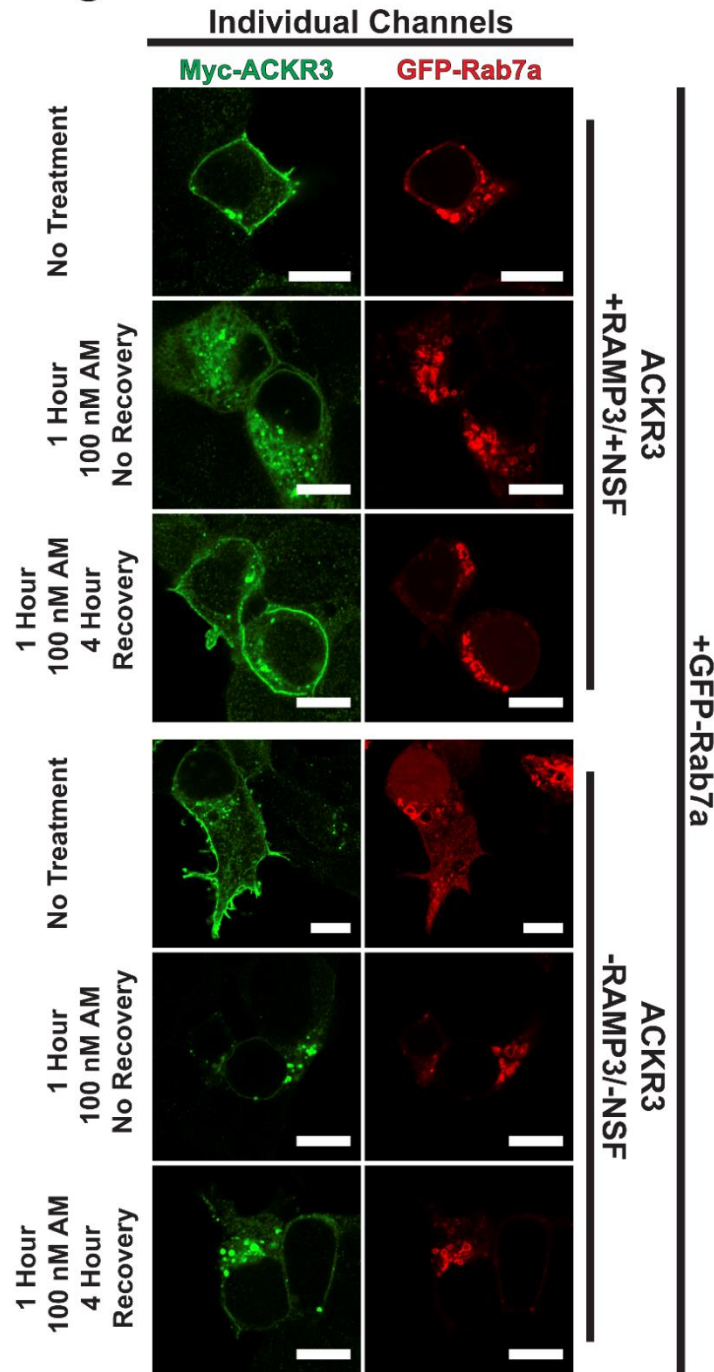


Fig. S7. Individual channels for each protein during ACKR3: RAMP3: Rab7a recycling experiments in figure 4B. HEK293T cells are transfected with ACKR3 \pm RAMP3/NSF and GFP-Rab7a then cultured overnight. Cells were either not treated with ligand and fixed, treated with AM for 1 h and fixed, or treated with AM for 1 h washed/ allowed to recover for 4 h, and fixed. The first column represents Myc-ACKR3 staining (green) and the second column represents GFP-Rab7a expression (red). Treatments and transfection conditions can be found on the left and right of images, respectively. Images are representative of 3 independent experiments. Scale bar 10 μ m.

Fig. S8

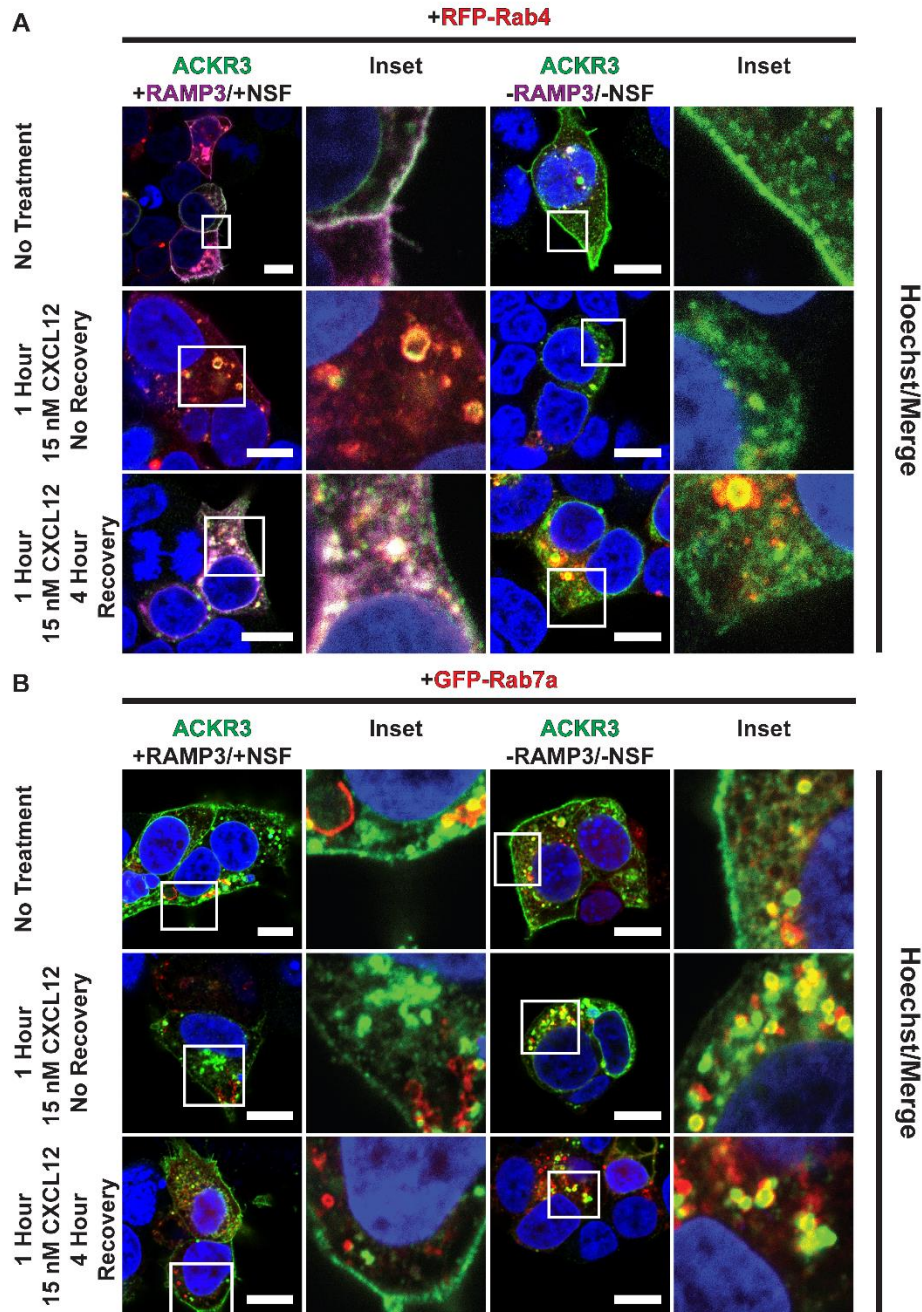


Fig. S8. ACKR3 binds CXCL12 leading to internalization and resensitization through Rab4 rapid recycling vesicles when co-expressed with RAMP3, ACKR3 resensitization is lost in the absences of RAMP3 through Rab7a late endosomes. (A) HEK293T cells transfected with RFP-Rab4 and ACKR3 \pm RAMP3/NSF were treated with 15 nM CXCL12 with the same method as figure 6. After 1 h CXCL12 treatment, ACKR3 +RAMP3/NSF are internalized and show colocalization with Rab4 intracellularly (middle row, first column and inset). In the ACKR3 – RAMP3/NSF condition, ACKR3 is internalized but colocalization with Rab4 does not occur (middle row, third column and inset). After a 4 h recovery time post-CXCL12 treatment, in the ACKR3 +RAMP3/NSF cells, ACKR3 and RAMP3 show distribution at the plasma membrane of the cell, demonstrating recycling of the receptor complex (bottom row, first column and inset). In the

ACKR3 –RAMP3/NSF cells, after the 4 h recovery, ACKR3 is not present at the plasma membrane and the receptor remained intracellular (bottom row, third column and inset). (B) Conversely, HEK293T cells transfected with GFP-Rab7a and ACKR3 ±RAMP3/NSF were treated with CXCL12. After 1 h CXCL12 treatment, ACKR3 +RAMP3/NSF are internalized and show no colocalization with Rab7a intracellularly (middle row, first column and inset). In the ACKR3 –RAMP3/NSF treated cells, ACKR3 is internalized and shows robust localization in the lumen of Rab7a-positive vesicles (middle row, third column and inset). After a 4 h recovery time post-CXCL12 treatment, in the ACKR3 +RAMP3/NSF cells, ACKR3 and RAMP3 show distribution at the plasma membrane of the cell, demonstrating recycling of the receptor complex (bottom row, first column and inset). In the ACKR3 –RAMP3/NSF cells, after the 4 h recovery, ACKR3 is not present at the plasma membrane but is detected in the lumen of Rab7a-late endosomes (bottom row, third column and inset). Images are representative of at least two independent experiments. Scale bar 10 μ m.

Fig. S9

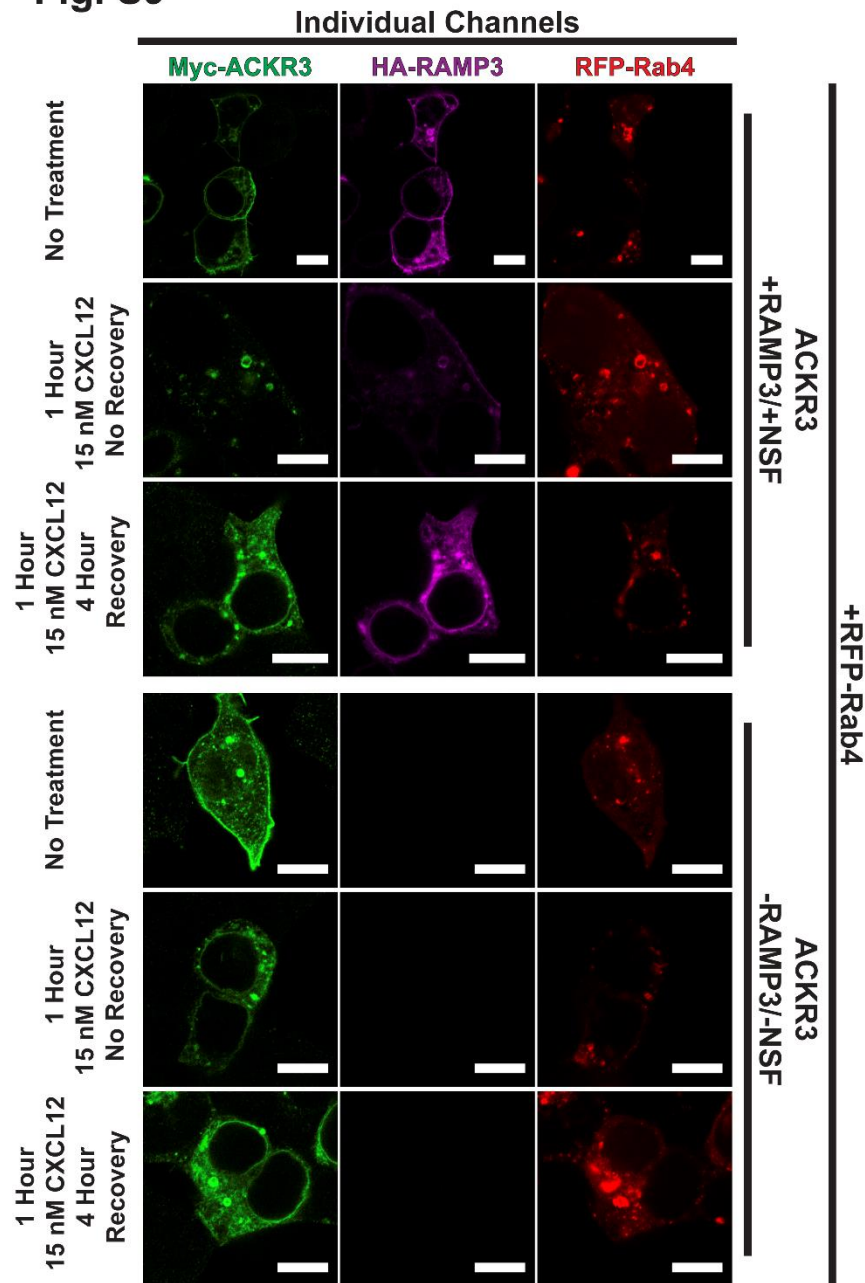


Fig. S9. Individual channels for each protein during ACKR3: RAMP3: Rab4 recycling experiments in figure S8A. HEK293T cells are transfected with ACKR3 \pm RAMP3/NSF and RFP-Rab4 then cultured overnight. Cells were either not treated with ligand and fixed, treated with CXCL12 for 1 h and fixed, or treated with CXCL12 for 1 h washed/ allowed to recover for 4 h, and fixed. The first column represents Myc-ACKR3 staining (green), the second column represents HA-RAMP3 staining (magenta), and the third column represents RFP-Rab4 expression (red). Treatments and transfection conditions can be found on the left and right of images, respectively. Images are representative of at least two independent experiments. Scale bar 10 μ m.

Fig. S11

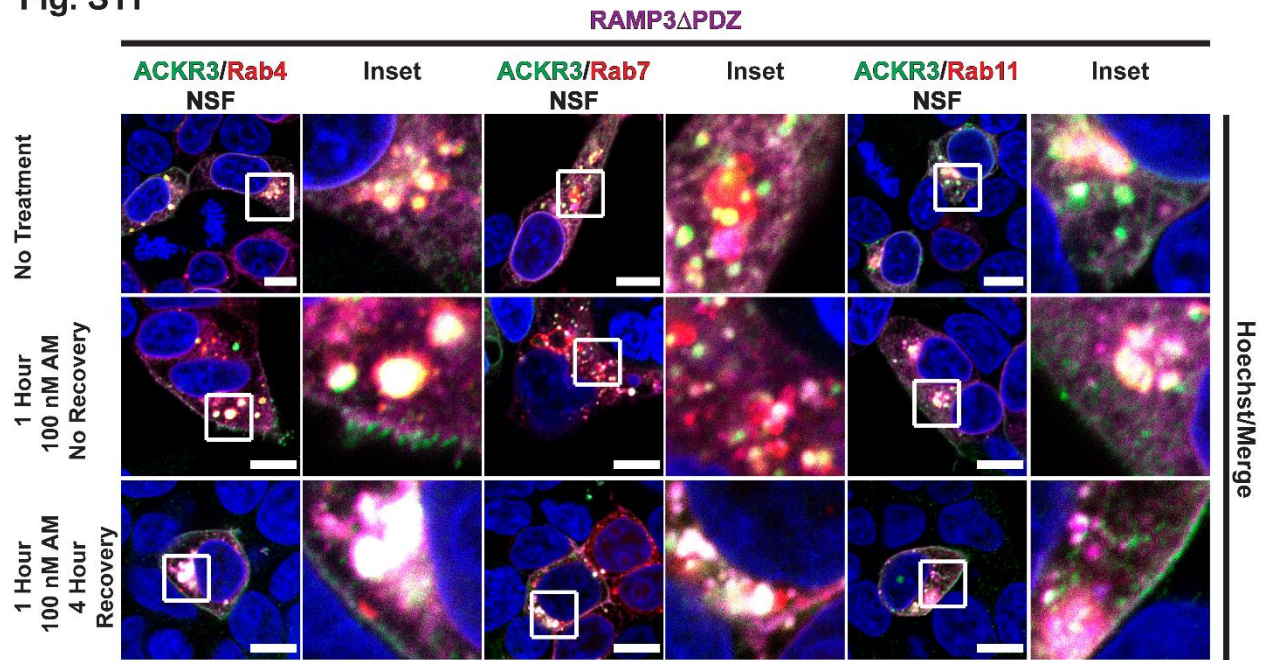


Fig. S11. Deletion of the RAMP3's type I PDZ results in the dysregulation of the ACKR3:RAMP3 complex during AM stimulation. (A) HEK293T cells transfected with Rab4, Rab7, or Rab11 and ACKR3 +RAMP3 Δ PDZ/NSF were not treated with AM, treated with 100 nM AM for 1 h and fixed, or treated and allowed to recover for 4 h. Under basal conditions, the deletion of the type I PDZ domain resulted in an increase in the receptor complex internalizing and interacting with all three Rabs, which was not previously detected with WT-RAMP3. After 1 h AM treatment, ACKR3 + RAMP3 Δ PDZ/NSF are internalized and show colocalization with all three Rabs intracellularly (middle row and insets). After a 4 h recovery time post-AM treatment, in the ACKR3 + RAMP3 Δ PDZ/NSF cells, ACKR3 and RAMP3 show distribution at the plasma membrane of the cell, as well as localizing to Rab4, 7, and 11 positive vesicles indicating an inability of the mutant RAMP3 to control the vesicular trafficking of the ACKR3: RAMP3 Δ PDZ/NSF complex (bottom row and insets). Images are representative of three independent experiments. Scale bar 10 μ m.

Fig. S12

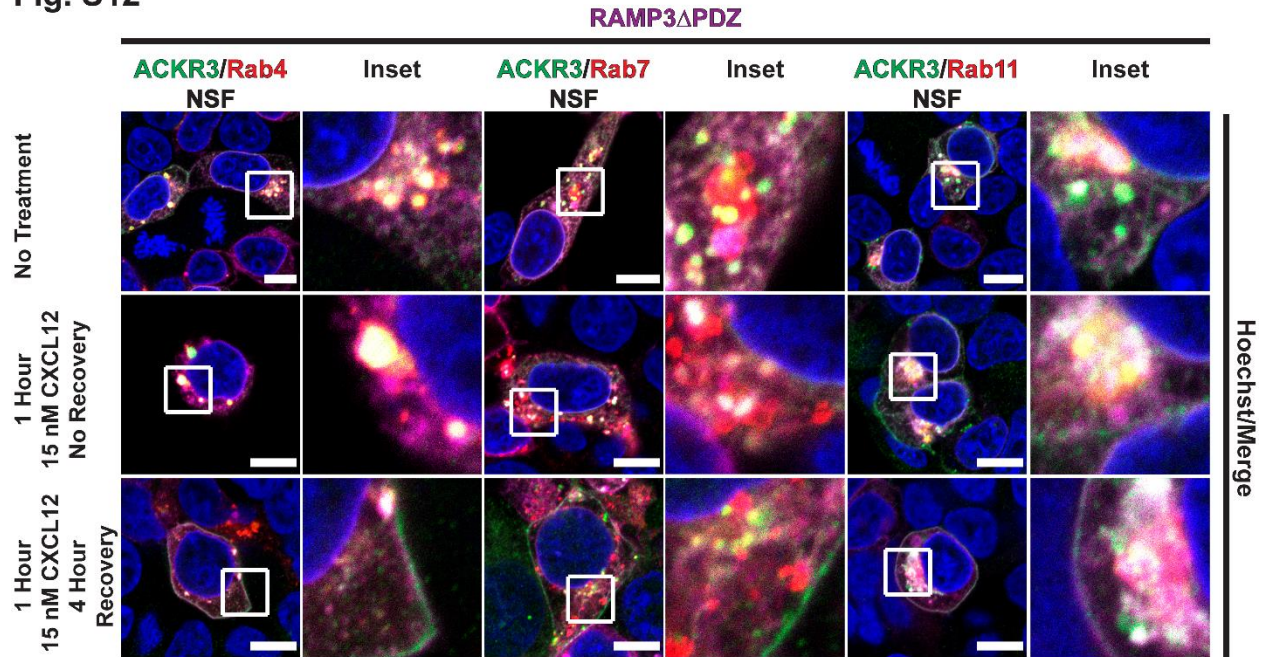


Fig. S12. Deletion of the RAMP3's type I PDZ results in the dysregulation of the ACKR3:RAMP3 complex during CXCL12 stimulation. (A) HEK293T cells transfected with Rab4, Rab7, or Rab11 and ACKR3 +RAMP3 Δ PDZ/NSF were not treated with CXCL12, treated with 15 nM CXCL12 for 1 h and fixed, or treated and allowed to recover for 4 h. Under basal conditions, the deletion of the type I PDZ domain resulted in an increase in the receptor complex internalizing and interacting with all three Rabs, which was not previously detected with WT-RAMP3. After 1 h CXCL12 treatment, ACKR3 + RAMP3 Δ PDZ/NSF are internalized and show colocalization with all three Rabs intracellularly (middle row and insets). After a 4 h recovery time post-AM treatment, in the ACKR3 + RAMP3 Δ PDZ/NSF cells, ACKR3 and RAMP3 show distribution at the plasma membrane of the cell, as well as localizing to Rab4, 7, and 11 positive vesicles indicating an inability of the mutant RAMP3 to control the vesicular trafficking of the ACKR3: RAMP3 Δ PDZ/NSF complex (bottom row and insets). Images are representative of three independent experiments. Scale bar 10 μ m.